On Building Blocks for Virtual Testing of Unidirectional Polymeric Composites

by

Joshua Robbins

A Thesis Presented in Partial Fulfillment
of the Requirements for the Degree
Master of Science

Approved November 2019 by the
Graduate Supervisory Committee:

Subramaniam Rajan, Chair
Barzin Mobasher
Christian Hoover

ARIZONA STATE UNIVERSITY

December 2019

ABSTRACT

This research summarizes the characterization of the constituent materials of a unidirectional composite for use in a finite element model. Specifically the T800s-F3900 composite from Toray Composites, Seattle, WA. Testing was carried out on cured polymer matrix provided by the manufacturer and single fiber specimen. The material model chosen for the polymer matrix was MAT 187 (Semi-Analytical Model for Polymers) which allowed for input of the tension, compression, and shear load responses.

The matrix was tested in tension, compression, and shear and was assumed to be isotropic. Ultimate strengths of the matrix were found to be 10 580 psi in tension, 25 900 psi in compression, and 5 940 in shear. The material properties calculated suggest the resin as being an isotropic material with the moduli in tension and compression being approximately equal (3% difference between the experimental values) and the shear modulus following typical isotropic relations. Single fiber properties were obtained for the T800s fiber in tension only with the modulus being approximately 40 500 ksi and the peak stress value being approximately 309 ksi.

The material model predicts the behavior of the multi-element testing simulations in both deformation and failure in the direction of loading.

DEDICATION

To my parents Deborah Busby and Sam Robbins without whom I would not be able to be where I am today and whose guidance and support has been immeasurable.

ACKNOWLEDGEMENTS

I would like to thank Dr. Rajan for his mentorship and guidance as my Committee Chair. I would also like to thank Dr. Hoover and Dr. Mobasher for serving as committee members and for the teaching they provided. I would like to thank Bilal Khaled and Loukham Shyamsunder for their guidance and mentorship. I would finally like to thank both Jeff Long and Peter Goguen for their help with laboratory procedures.

TABLE OF CONTENTS

Page

CHAPTER Page

LIST OF TABLES

Table Page

LIST OF FIGURES

Figure Page

Figure Page

Figure Page

1. Overview

1.1 Introduction

This research summarizes (a) the experimental procedures used to classify the behavior of the constituent materials of a unidirectional composite (T800s fibers and F3900 matrix from Toray Composites, Seattle, WA) and (b) implementing these material properties and responses in a predictive finite element model that can then be used to model the behavior of the constituents which was done to build towards a virtual test model for the composite. All tests were performed at quasi-static (QS) rates and at room temperature (RT). The tests on the epoxy matrix were performed in tension, compression, shear. The fiber was only tested in tension. The material model chosen was MAT 187 which is documented in Kolling, et al. (Kolling, Haufe, Feucht, & Dubois, 2005) and is summarized in chapter 6.1.

2. Literature Review

The testing of polymers to determine mechanical properties that can be used in a finite element model are standardized. When testing at quasi-static rates and at room temperature the American Society for Testing of Materials (ASTM) standard D638 (D20 Committee, n.d.-c, p. 638) suggests long dog bone specimen geometries for obtaining the tensile properties of plastics. When testing under compression, ASTM standard D6641 (D20 Committee, n.d.-a) can be used which was developed by Adams and Welsh (Adams, Donald, 1997) for use on composite laminates. This method was developed to allow for thin specimens of a differing gage length that can be supported while under compression and prevent buckling of the specimen. This standard gage length was suggested to be approximately 0.5 in. This method also tries to prevent the stress concentrations generated by tabbed specimens that are used in wedge-grip type loading methods. Liu and Piggott (Liu & Piggott, 1995) use the Isopescu shear (ASTM D5379 (D30 Committee, n.d.)) and punch shear tests (ASTM D732 (D20 Committee, n.d.-b)) to obtain the shear properties for a variety of thermoplastics at a range of temperatures from 20˚ to 120˚ C. They also noted that the shear punch test may not have been in pure shear because the failure surface of the polymers were not straight and there was no single failure of the specimen, often multiple peaks were reached. This also provided a comparison between the two tests.

Single fiber testing is explored in Langston and Granata (Langston & Granata, 2014) which followed ASTM D3379 (D30 Commitee, 1975) which used a tabbed method with the fiber affixed to the tab (described as a thin compliant material such as paper or

plastic) with a free gage section in the center that is then cut away allowing for direct tension of the specimen, however this standard was retired. Similarly, Kim et al (Kim, McDonough, Blair, & Holmes, 2008) used ASTM C1557 (C28 Committee, n.d.) which describes a similar technique to the previous standard with the only difference being the gripping method being rigid pins instead of a clamping method. The diameter of fibers for both these methods was anywhere from 1 to 250 μm.

3. General Experimental Test Procedures

3.1 Sample Preparation

A waterjet was used to cut the samples. The waterjet specifications are shown in Table 3.1 Specifications of the abrasive used in the waterjet are shown in Table 3.2.

3.1 Waterjet Specifications

	16-ply Samples	**24-ply Samples**	**96-ply Samples**
Approximate Thickness (in)	0.125	0.182	0.728
Abrasive Size (grit)	80 (US Std)	80 (US Std)	80 (US Std)
Nozzle Diameter (in)	0.03	0.03	0.03
Minimum Nozzle Pressure (psi)	30000	30000	30000
Maximum Nozzle Pressure (psi)	45000	45000	45000
Cut Speed (in/min)			
Quality 1	135.43	94.3	21.42
Quality 2	116.15	80.88	18.37
Quality 3	72.87	50.74	11.53
Quality 4	52.34	36.45	8.28
Quality 5	40.5	28.2	6.41

3.2 80-Grit (US Std) Specifications

Sieve Size (US Std)	Sieve Mesh Diameter (in)	% Retained
8	0.0937	0
12	0.0661	0
14	0.0555	0
16	0.0469	0
20	0.0331	0
30	0.0234	0
40	0.0165	0-5
50	0.0117	10-35
60	0.0098	20-40
80	0.007	20-50
120	0.0049	0-15
Pan	-	0-3

A typical panel before being cut is shown in Fig. 3.1 and a typical panel after being cut is shown in Fig. 3.2.

3.1 Epoxy Panel Before Cutting

3.2 Epoxy Panel After Being Cut

All specimens, unless stated otherwise, were painted and speckled as follows. The gage section was painted with a thin layer of white paint with a flat finish. After the white

paint had dried, black paint with a flat finish, was sprayed onto the white paint in such a manner that it created a random distribution of black dots until approximately fifty percent of the white area was covered in black paint. A close-up of a typical speckled surface is shown in Fig. 3.3.

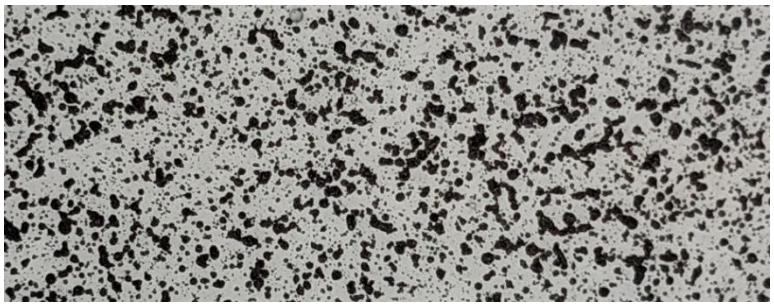

3.3 Close Up of A Typical Speckled Surface

3.2 Test Machines, Fixtures, Equipment and Software

All tests for the matrix were performed on an MTS-810 universal test frame[1]. Load was captured in the FlexTest SE Station Manager Version 5.1B 2592 software and were measured using an MTS 20-kip Load Cell Model #661.21A-03. An overall view of the test frame can be seen in Fig. 3.4.

[1] https://www.mts.com/en/products/producttype/test-systems/load-frames-uniaxial/servohydraulic/standard/index.htm

3.4 MTS-810 Test Frame

3.5 Typical DIC Camera Setup

Digital Image Correlation (DIC) was used to capture the deformations and strains of the specimens using VIC-Snap version 8 Build 289 (“Correlated Solutions Inc,” 2016) at a rate of 1 picture every second during both the shear and compression tests and a rate of 1 picture every two seconds for the tension tests. A typical setup for the cameras can be seen in Fig. 3.5 during the Isopescu shear test, the only difference between different tests being the lighting placement and camera height.

Two Point Grey Grasshopper 3[2] cameras were used to capture images of the specimen throughout the duration of the experiment. LED lamps were used to properly illuminate the specimen during the experiment. The cameras and lights were fixed to the same frame. The frame is leveled using a bubble level in order to ensure the field of view of the cameras is both horizontal and vertical respectively.

[2] https://www.ptgrey.com/grasshopper3-gige-vision-cameras

3.3 Typical Test Procedure

The procedure for each test conducted in this study was the same unless noted otherwise. Prior to each test the Vic-3D 7 system was calibrated once the cameras were in place, leveled, and focused. The calibration files were then used for each replicated unless the camera system was moved or the specimen plane was moved due to a change in test fixture. All specimens were loaded in displacement control.

3.4 Post-processing of Test Data

The force being transmitted through the specimen was obtained using the load cell attached to the testing frame. The compressive and tensile stresses were calculated using

$$\sigma = \frac{F}{A} \tag{4.1}$$

where σ is the axial stress, F is the axial force, and A is the initial cross-sectional area of the specimen. The shear stresses were calculated using

$$\tau = \frac{F}{A} \tag{4.2}$$

where τ is the shear stress, F is the force reported by the load cell, and A is the initial cross-sectional area of the specimen between the notches. Specimen dimensions were measured using a Pittsburgh 4" Digital Caliper[3]. The caliper has a resolution of 0.0005 in.

Strain data was processed with the Vic-3D 7 software version 7.2.6 Build 449. Pixel resolution was 2448 by 2048 in the field of view with an approximate pixel density of 410 pixels/inch. For the initial processing, the entire speckled region of the specimen

[3] https://www.harborfreight.com/4-in-Digital-Caliper-63710.html

was analyzed. The Lagrangian strain tensor was chosen during the initial analysis, which was then smoothed by the Vic-3D software internally. The strain was smoothed using a decay filter algorithm. After the analysis and smoothing were completed, a smaller region was taken as the representative strain induced in the specimen for both the tension and shear specimens. The compression specimens were analyzed using the average strain over the whole analyzed region. Typically, these regions are away from the edges of the specimen where strain concentrations may occur especially where the specimen is gripped. Typical sample regions are shown in Figs. 3.6, 3.7, and 3.8

4. F3900 Matrix Experimental Test Details and Results

4.1 Overview

4.2 F3900 Matrix Tension Test

Specimen Geometry: The specimen dimensions and geometry, shown in Fig. 4.1, are taken from ASTM D638-14 (2014) for a Type II specimen to promote failure in the gage section.

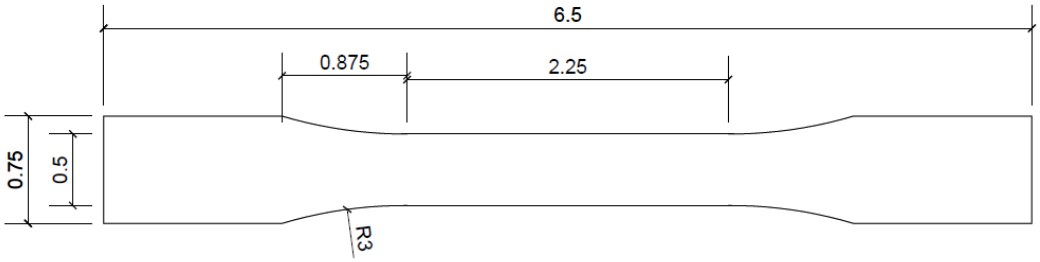

4.1 Typical Specimen Geometry and Layout (Dimensions in Inches)

The average specimen dimensions in the gage section are shown in Table 4.1.

4.1 Tension Test Specimen Dimensions

Replicate	Width (in)	Thickness (in)	Cross Sectional Area (in^2)
ET-4	0.505	0.147	0.0741
ET-5	0.504	0.145	0.0731
ET-6	0.504	0.145	0.0730
ET-7	0.504	0.150	0.0755
Average	0.504	0.147	0.0742
Std. Dev.	0.0005	0.00236	0.00121
Coeff of Var.	0.1%	1.6%	1.6%

Test Machines, Fixtures, Equipment, and Software: Tension tests were performed using MTS 647.10A hydraulic grips and were loaded in displacement control at a rate of 0.01 in/min. A typical test setup for the tension specimens can be seen in Fig. 4.2. After

manually aligning the hydraulic grips, the specimen was placed into the test frame. Verticality of the specimen was assured by a laser alignment system. The specimen was then gripped on the either edge for the first 1.25 in. The specimens were then gripped with a hydraulic gripping pressure of 200 psi.

4.2 Typical Tension Test Setup

Specimen Photographs: The specimen photographs before the tests are shown in Fig. 4.3. The specimens exhibited brittle failure of the matrix before the tests were terminated. Fig. 4.4 shows the specimens after testing.

(a)

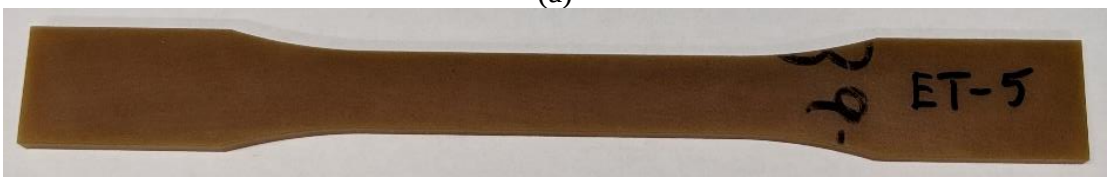

(b)

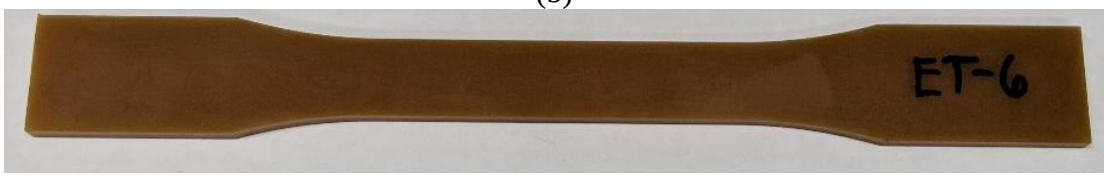

(c)

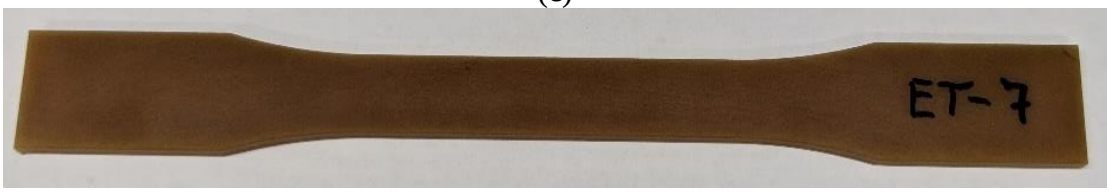

(d)

4.3 Specimens (a) ET-4, (b) ET-5, (c) ET-6, and (d) ET-7 Pretest

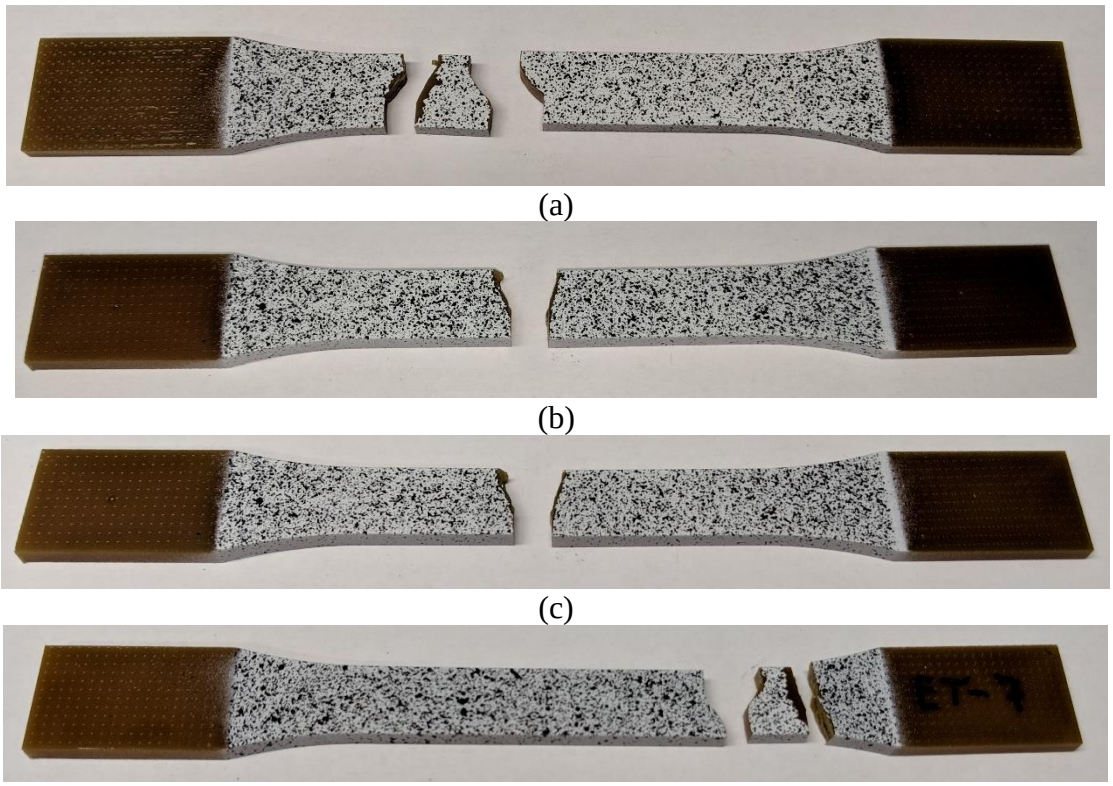

(a)

(b)

(c)

(d)

4.4 Specimens (a) ET-4, (b) ET-5, (c) ET-6, and (d) ET-7 Posttest

Test Results: The summary of the results from the tests are shown in Table 4.2.

4.2 Tension Test Results Summary

Replicate	**Loading Rate (in/min)**	**Strain Rate** $\left(s^{-1}\right)$	**E_{22} (psi)**	**Poisson's Ratio (ν)**	**Ultimate Strain**	**Peak Stress (psi)**
ET-4	0.01	$4(10)^{-5}$	409 000	0.389	0.0316	10 300
ET-5	0.01	$4(10)^{-5}$	412 000	0.386	0.0341	10 800
ET-6	0.01	$4(10)^{-5}$	406 000	0.386	0.0334	10 630
ET-7	0.01	$4(10)^{-5}$	410 000	0.387	0.0332	10 570
Average	-	-	409 000	0.387	0.0331	10 580
Standard Deviation	-	-	2 190	0.0014	0.0011	197
Coefficient of Variation	-	-	0.5%	0.3%	3.2%	1.9%

The strain rate data was obtained from the DIC results and is an average value over the duration of the test. Poisson's ratio was obtained by plotting the transverse strain against the longitudinal strain and performing a linear regression. The slope of the fitted equation was then taken as Poisson's ratio for the specimen.

Fig. 4.5 shows the stress-strain curves for the four replicates as well as an average curve (designated the *Model Curve*) which will be used as an input into the finite element model. For comparison with the T800S/F3900 composite, Fig. 4.5 shows the 2-direction (in-plane, transverse to unidirectional fibers) tension model curve since the epoxy matrix likely dominates the deformation and failure mechanisms in this loading state.

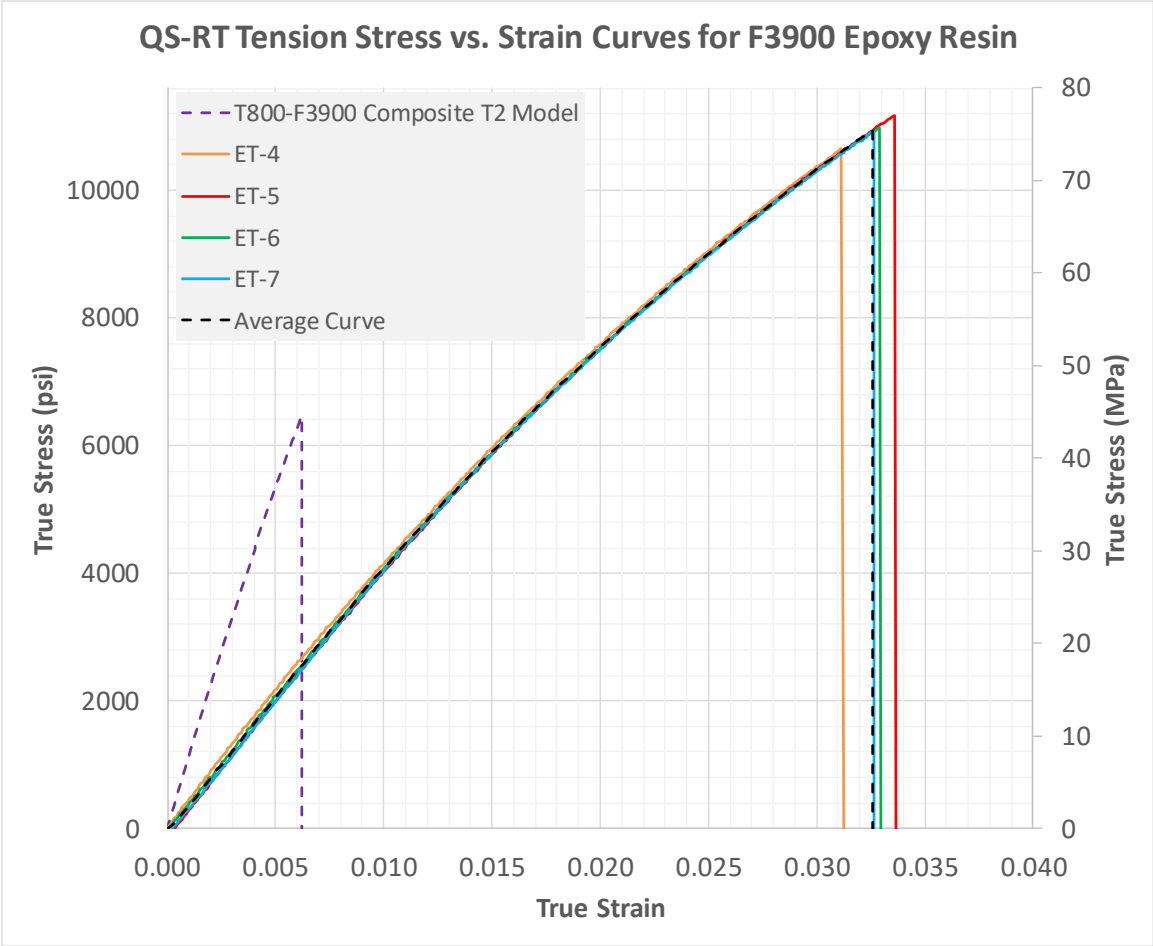

4.5 Engineering Stress vs. Lagrangian Strain Curve for The Tension Tests

Use in Finite Element Model: The Model Curve is used to create the MAT187 card under the input variable LCID_T. This curve is the plastic strain vs. yield stress curve with the plastic strain defined as

$$\varepsilon_{pt} = \varepsilon_t - \frac{\sigma_t}{E} \tag{5.1}$$

where σ_t is the tensile stress at a given point *t*, ε_t is the Lagrangian longitudinal total strain obtained from DIC, and E is the average elastic modulus of the replicates. The curve was smoothed using 11 point moving average with 5 runs of smoothing done. Figure 4.6 shows the Model Curve adjusted to show stress vs. plastic strain.

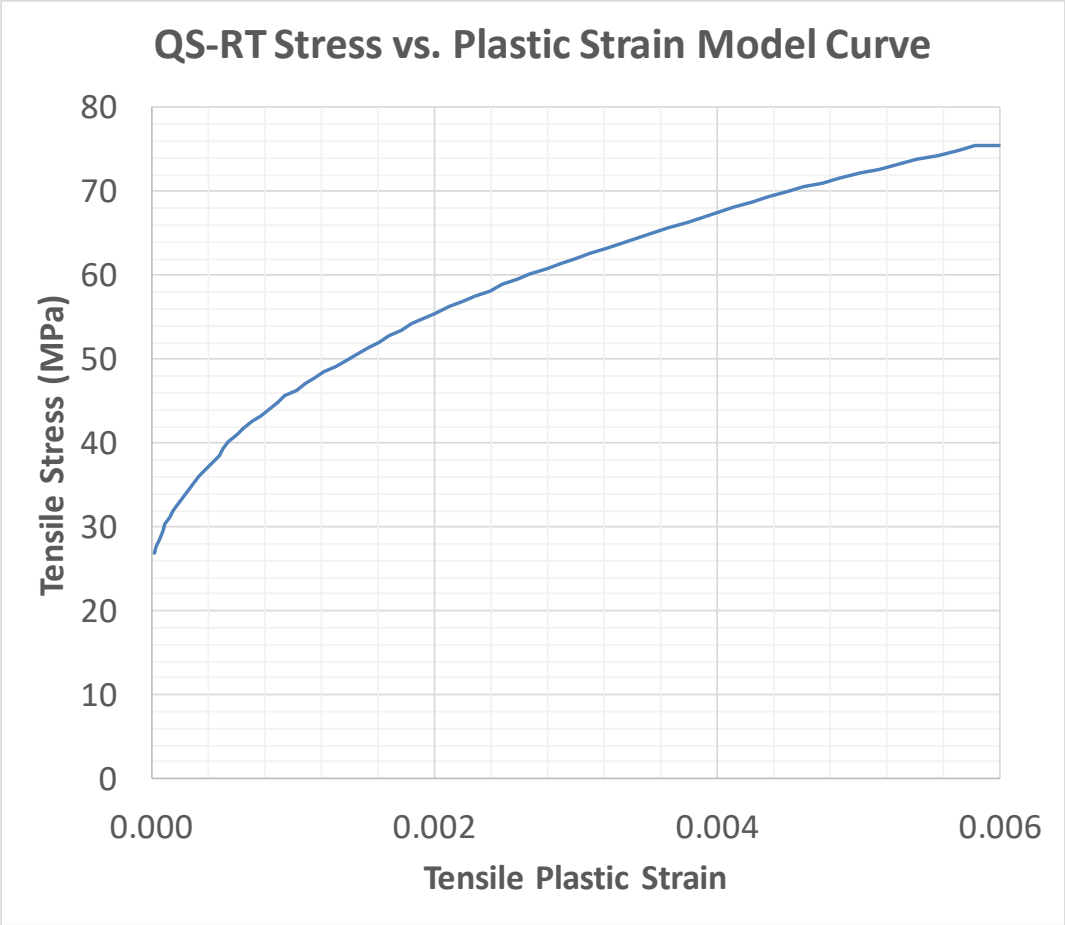

4.6 Stress vs. Plastic Strain Model Curve for Finite Element Models

The last point of the tension model input curve is extrapolated at the same stress value. This is done because LS-DYNA will extrapolate all input curves based on the last two points of the input which can then result in simulations behaving in a manner outside what is prescribed by the input. Therefore the curves are extrapolated at the final stress value to ensure that the stresses in a given material direction do not exceed the maximum values observed during the experiment.

4.3 F3900 Matrix Compression Test

Specimen Geometry: Specimen dimensions and geometry are shown in Fig. 4.7 which are taken from ASTM D6641-16e1 (2016).

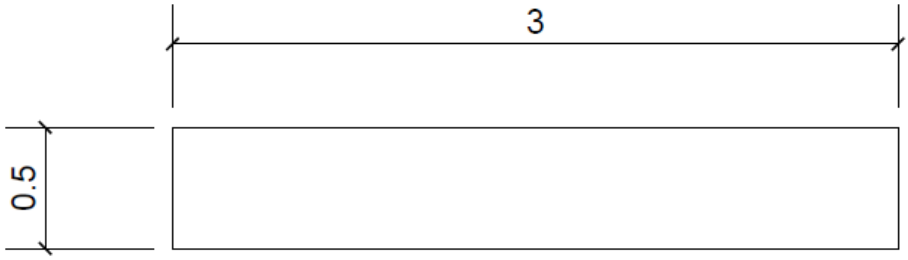

4.7 Typical Specimen Geometry and Layout (Dimensions in Inches)

The average specimen dimensions in the gage section are shown in Table 4.3.

4.3 Compression Test Specimen Dimensions

Replicate	Width (in)	Thickness (in)	Cross Sectional Area (in2)
EC-4	0.504	0.161	0.0813
EC-5	0.504	0.160	0.0807
EC-6	0.503	0.162	0.0803
EC-7	0.504	0.150	0.0758
EC-8	0.503	0.158	0.0793
Average	0.504	0.158	0.0795
Std. Dev.	0.00055	0.0048	0.0022
Coeff of Var.	0.1%	3.0%	2.7%

Test Machines, Fixtures, Equipment, and Software: Specimens were centered and placed in a Combined Loading Compression (CLC) fixture[4] with an exposed gage height of 0.5 in. Proper placement of the specimen into the fixture was ensured with two machined parallel plates each of 0.5 in width (Fig. 4.8). The top of the fixture was then placed on top with the two parallel plates still in place (Fig. 4.9). The bolts of the CLC

[4] http://www.wyomingtestfixtures.com/Products/b1.html

fixture were then finger tightened to ensure the specimen would not move after which the alignment plates were removed. The bolts were then tightened with a torque of 13 lb-in verified with a digital torque wrench. Specimens were loaded in displacement control at a rate of 0.025 in/min (Fig. 4.10). Fig. 4.11 shows the CLC fixture in the test frame.

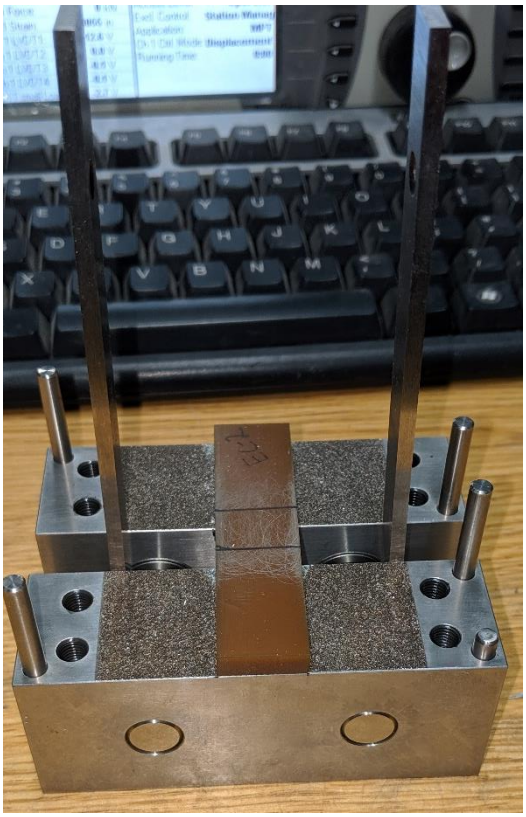

4.8 Specimen Centered on Bottom Half of Fixture with Alignment Plates

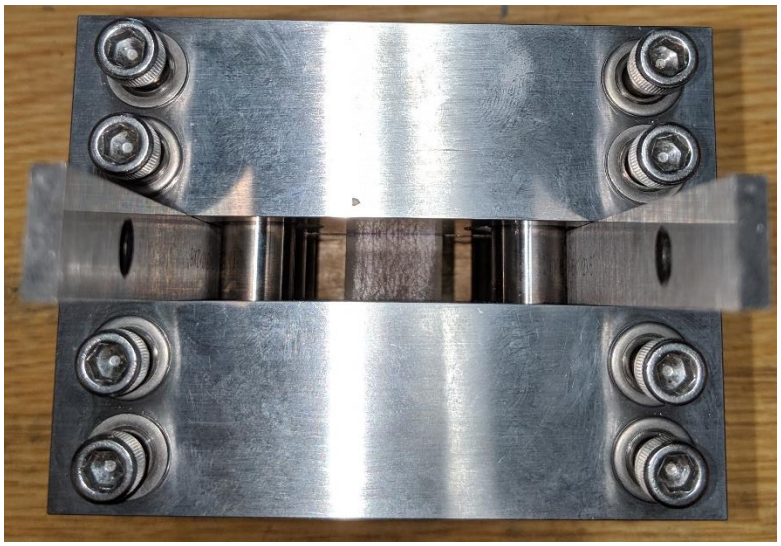

4.9 Fixture Assembled with Specimen Inside and Alignment Plates

4.10 Fixture Tightened with Digital torque Wrench Used

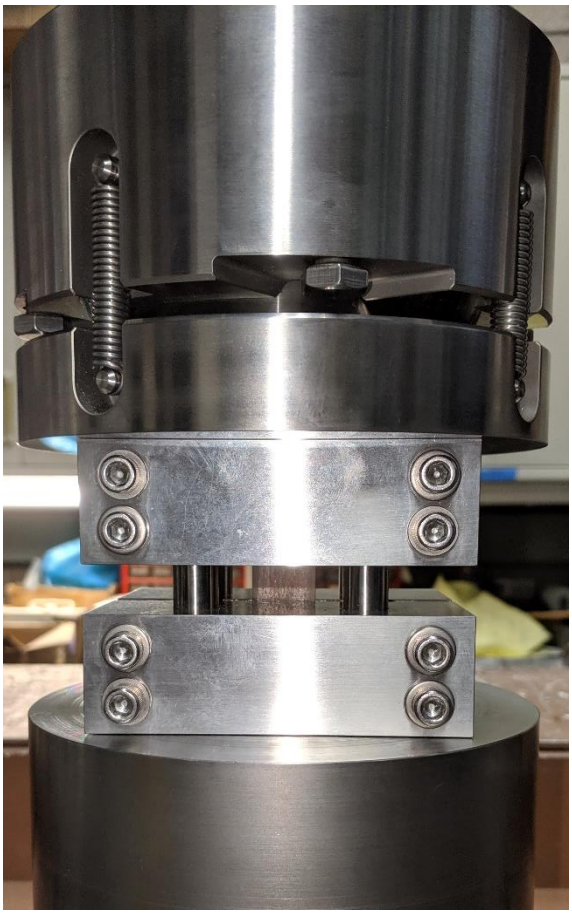

4.11 Fixture in Test Frame

Specimen Photographs: The specimen photographs before the tests are shown in Fig. 4.12. Fig. 4.13 shows the specimens after testing.

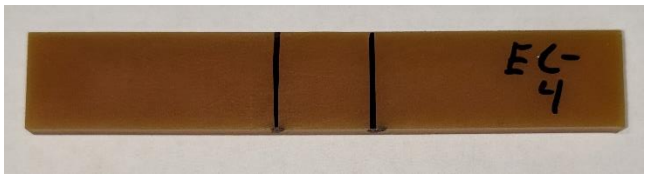

(a)

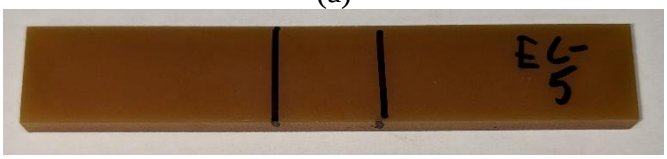

(b)

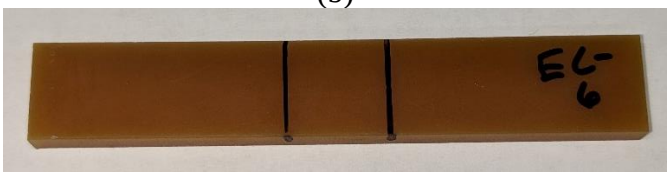

(c)

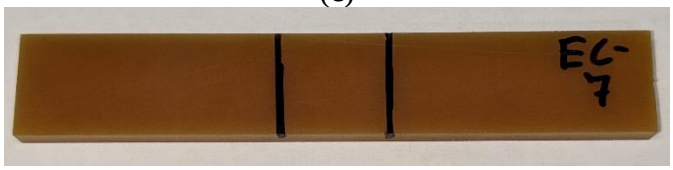

(d)

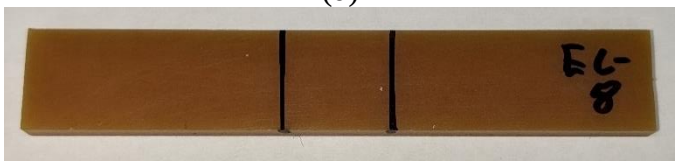

(e)

4.12 (a) EC-4, (b) EC-5, (c) EC-6, (d) EC-7, and (e) EC-8 Compression Specimens Pretest

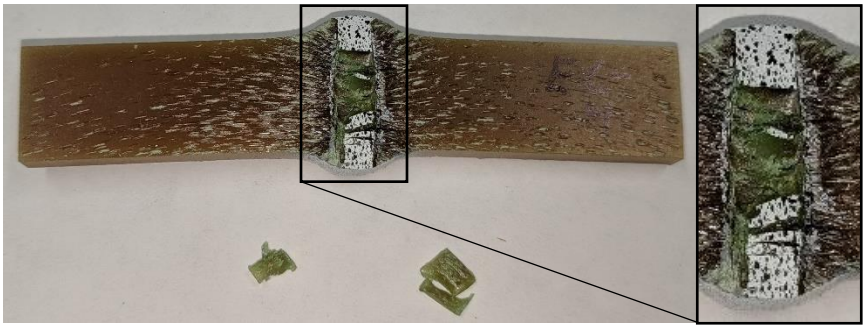

(a)

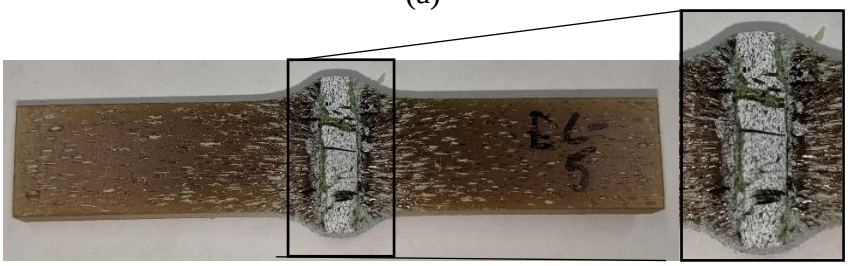

(b)

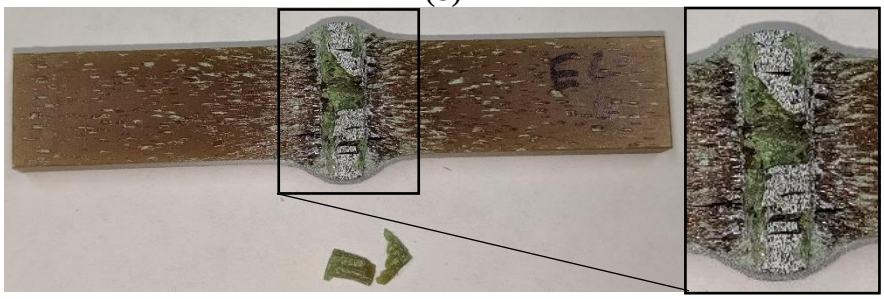

(c)

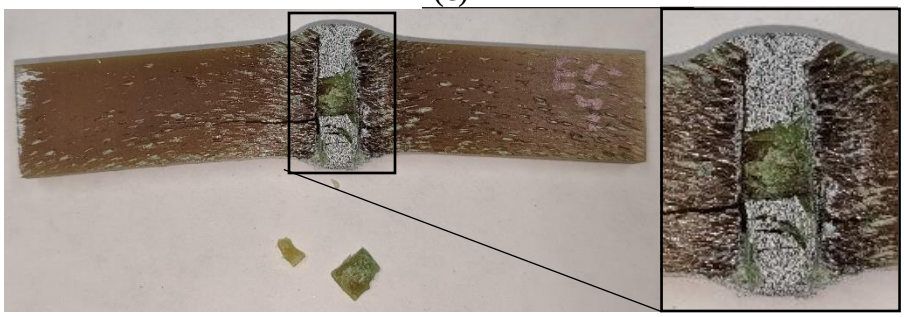

(d)

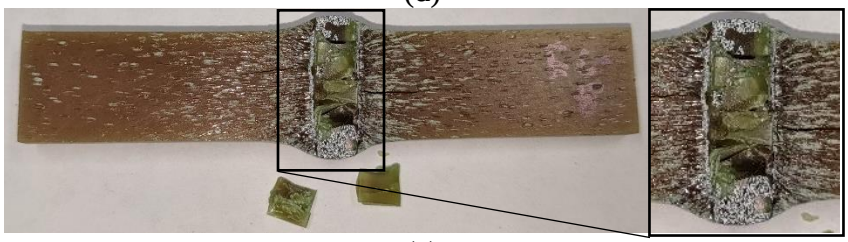

(e)

4.13 (a) EC-4, (b) EC-5, (c) EC-6, (d) EC-7, and (e) EC-8 Compression Specimens Posttest with Closeups of the Gage Section Where Barreling Occurs

Test Results: Fig. 4.14 shows the individual engineering stress vs. Lagrangian strain curves for the specimens. It can be observed that after the strains reach about 12-15%, the specimen strength begins to plateau and the stiffen with further loading. This is consistent with data from Littel (Littell, 2008) where specimens of a similar polymer matrix exhibited the same type of deformation and failure when loaded in compression.

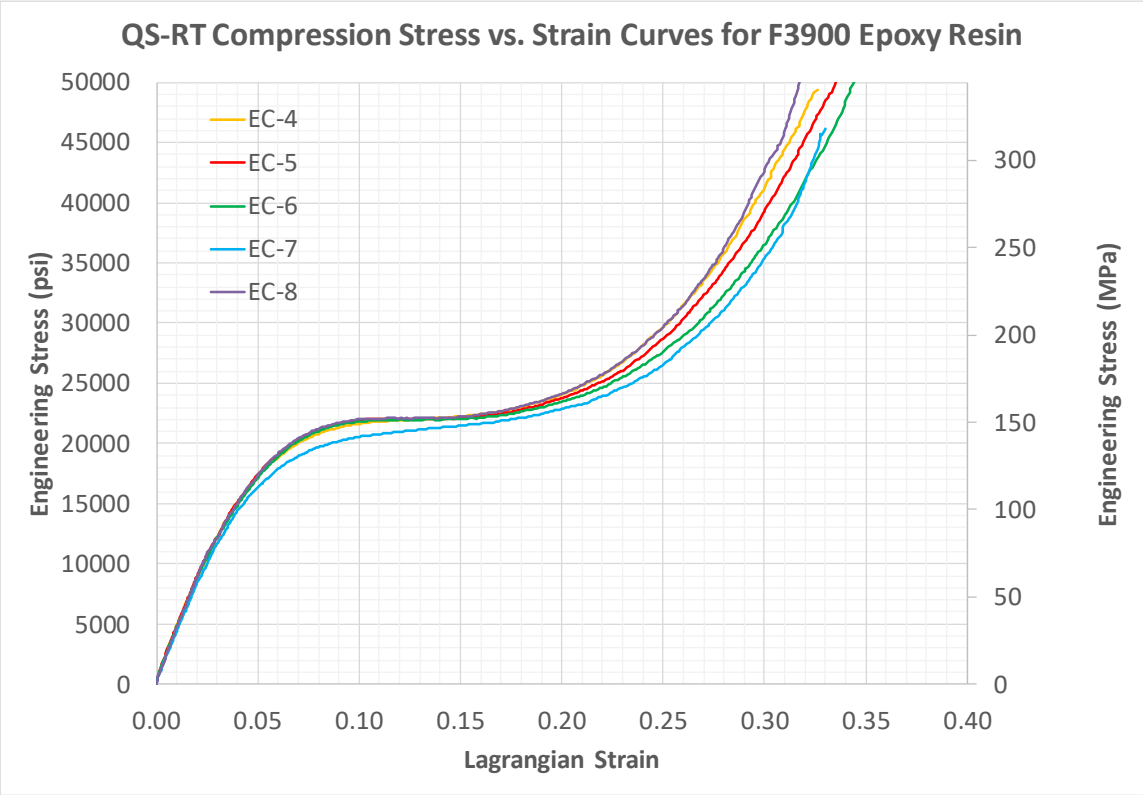

4.14 Engineering Stress vs. Lagrangian Strain Curve for Compression Tests

The compression curves were converted into the true stress - true strain space using the following equations with the assumption of volume constancy:

$$\varepsilon_T = \ln\left(1+\varepsilon_{yy}\right) \tag{5.2}$$

$$\sigma_T = \sigma_{eng}\left(1+\varepsilon_{yy}\right) \tag{5.3}$$

where ε_{yy} is the longitudinal strain and σ_{eng} is the calculated engineering strain using equation 1.1. A model input curve was generated using the replicate data up to the point where the specimens began to barrel out (approximate strain of 0.12). At this point during the experiments, the DIC data became less reliable since the analysis field began to shrink in size. Additionally, when the specimen begins to barrel out, decoupling the effects of geometry and material behavior on the stress-strain response becomes challenging. Even using the true stress definition, under the assumption of volume constancy, may not completely remove the geometric contribution from the response thus necessitating the need to cut off the data prior to the geometric effect becoming prominent. Fig. 4.15 shows a DIC image corresponding to the beginning of the barreling process during the procedure. The true stress vs. true strain curves are shown in Fig. 4.16 including the Model Curve. Table 4.4 shows a summary of the data.

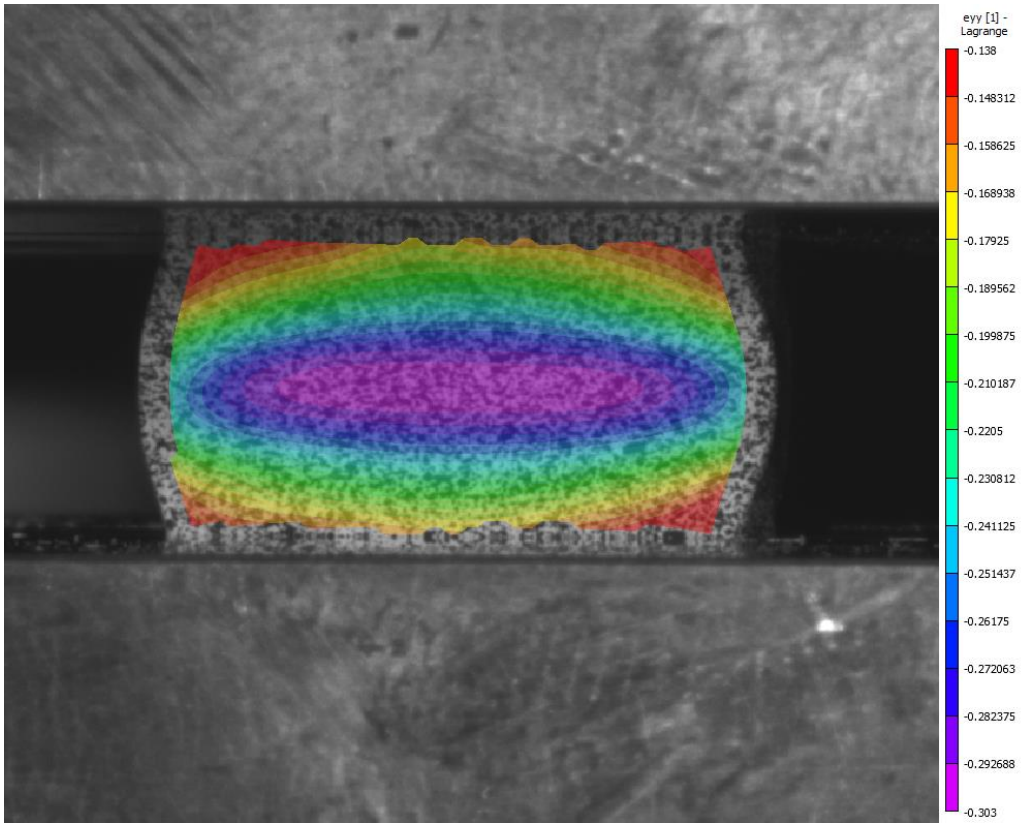

4.15 DIC Strain Field at the End of True Stress vs. True Strain Curve (EC-6)

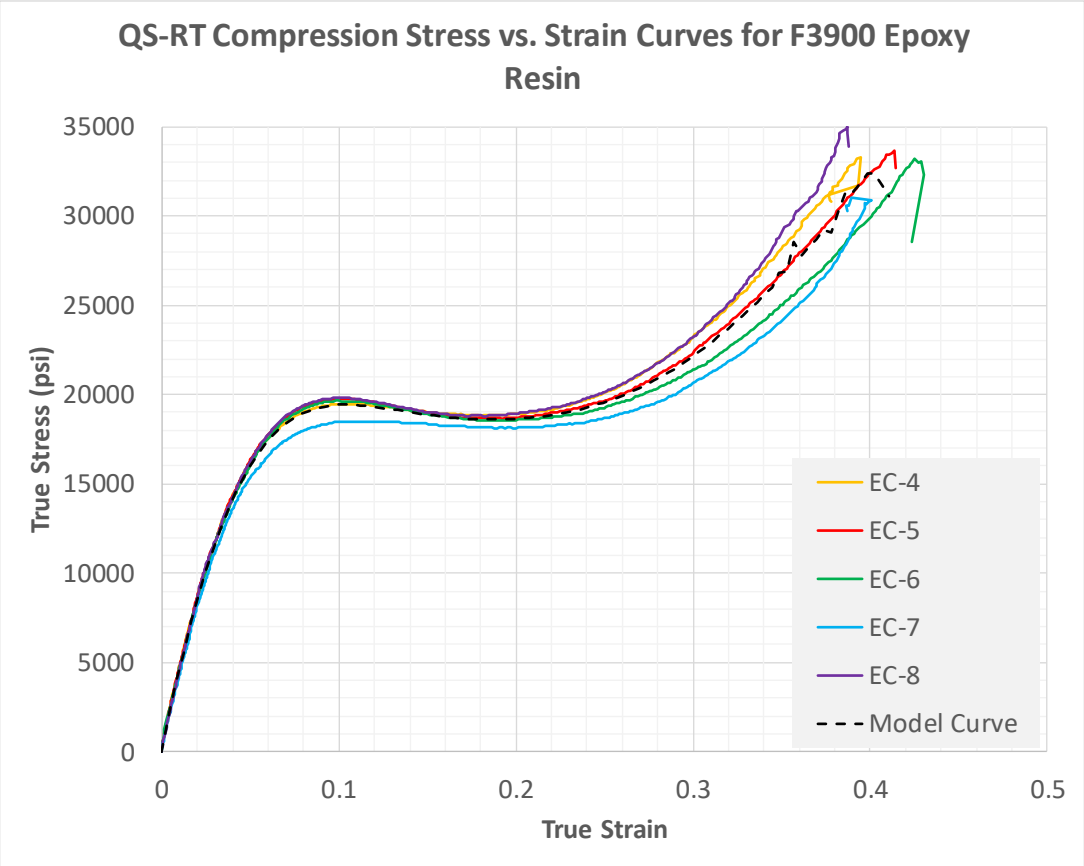

4.16 True Stress vs. True Strain Curve for Compression Tests

4.4 Compression Test Data Summary

Replicate	**Loading Rate (in/min)**	**Strain Rate** $\left(s^{-1}\right)$	**E_{22} (psi)**	**Elastic Poisson's Ratio (v)**
EC-4	0.025	$4(10)^{-4}$	433 000	0.484
EC-5	0.025	$4(10)^{-4}$	426 000	0.503
EC-6	0.025	$2(10)^{-4}$	406 000	0.505
EC-7	0.025	$2(10)^{-4}$	409 000	0.506
EC-8	0.025	$2(10)^{-4}$	438 000	0.510
Average	-	-	422 000	0.502
Standard Deviation	-	-	14 500	0.0102
Coefficient of Variation	-	-	3.4%	2.0%

Use in Finite Element Model: The Model Curve is used to create the MAT187 card under the input variable LCID_C. This curve is the plastic strain vs. yield stress curve with the plastic strain defined as

$$\varepsilon_{pc} = \varepsilon_c - \frac{\sigma_c}{E} \tag{5.4}$$

where σ_c is the compressive stress at a given point, ε_c is the Lagrangian compressive strain obtained from DIC, and E taken as the average compressive modulus of the replicates. The curve was then smoothed in a similar fashion as the tension curve. Figure 4.17 shows the Model Curve.

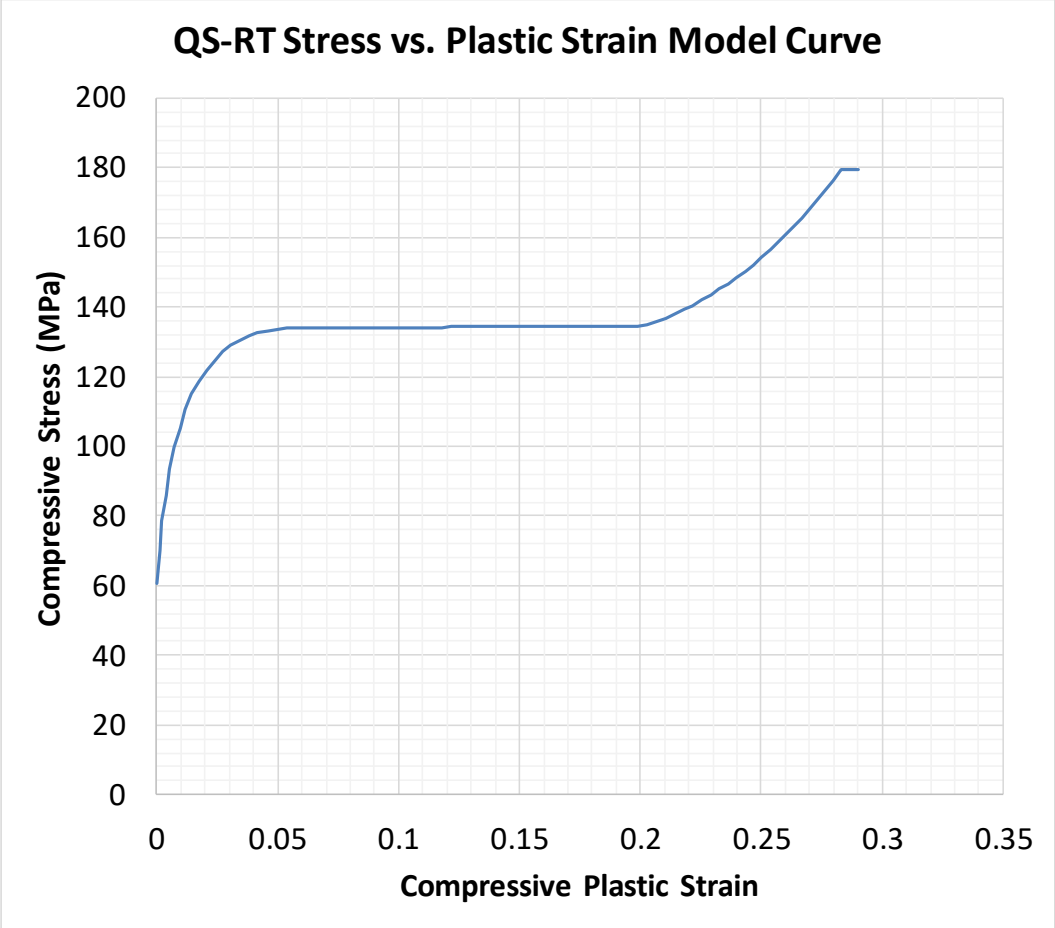

4.17 Model Input Curve for Compressive Plastic Strain vs. Compressive Stress

Similar to the Tension Model Curve, the last stress value is included again at a slightly higher strain since LS-DYNA will extrapolate the curve based on the last two points of the curve. This ensures that the material will not reach a higher stress than what was observed in the experiment.

4.4 F3900 Matrix Shear V-Notch Test

Specimen Geometry: Specimens were prepared in accordance with ASTM D5379 (2012) with the geometry shown in Fig. 4.18.

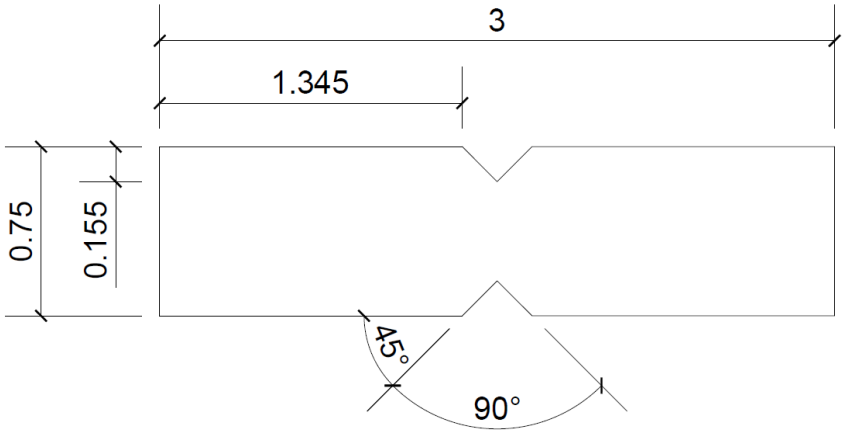

4.18 Typical V-notch Shear Specimen Geometry (Dimensions in Inches)

The average specimen dimensions in the gage section are shown in Table 4.5.

4.5 Shear Test Specimen Dimensions

Replicate	Width (in)	Thickness (in)	Cross Sectional Area (in^2)
ESV-6	0.451	0.154	0.0694
ESV-8	0.451	0.159	0.0717
ESV-9	0.448	0.157	0.0704
Average	0.450	0.157	0.0705
Std. Dev	0.0017	0.0025	0.0012
Coeff of Var.	0.4%	1.6%	1.6%

Specimen Preparation: Specimens were tabbed with G10 fiberglass tabs[5] in accordance with ASTM D5379 to prevent out of plane warping and to ensure the method of failure was purely shear and no bending was exhibited during the test. The tabs were machined to 0.75” by 1.25” per ASTM D5379 leaving a half inch gage section free to shear between the tabs. The tabs and the specimen surface where the tabs were to be bonded were abraded using a 120-grit sandpaper. The surfaces were then cleaned using an isopropyl alcohol-soaked cotton swab and allowed to air dry until there was no visible moisture. Then 3M Scotch-Weld 08966 Epoxy was mixed in accordance with the manufacturer’s specifications and applied in a thin layer on the prepared surface of the tabs using a wooden applicator. The tabs were then placed on the specimen and aligned using the tool shown in Fig. 4.19 and allowed to cure for at least 24 hours.

[5] G10, FR4 Laminate Sheets 36"x 48", Epoxyglas™; NEMA Grade FR4, Mil-I-24768/27, http://www.acculam.com/

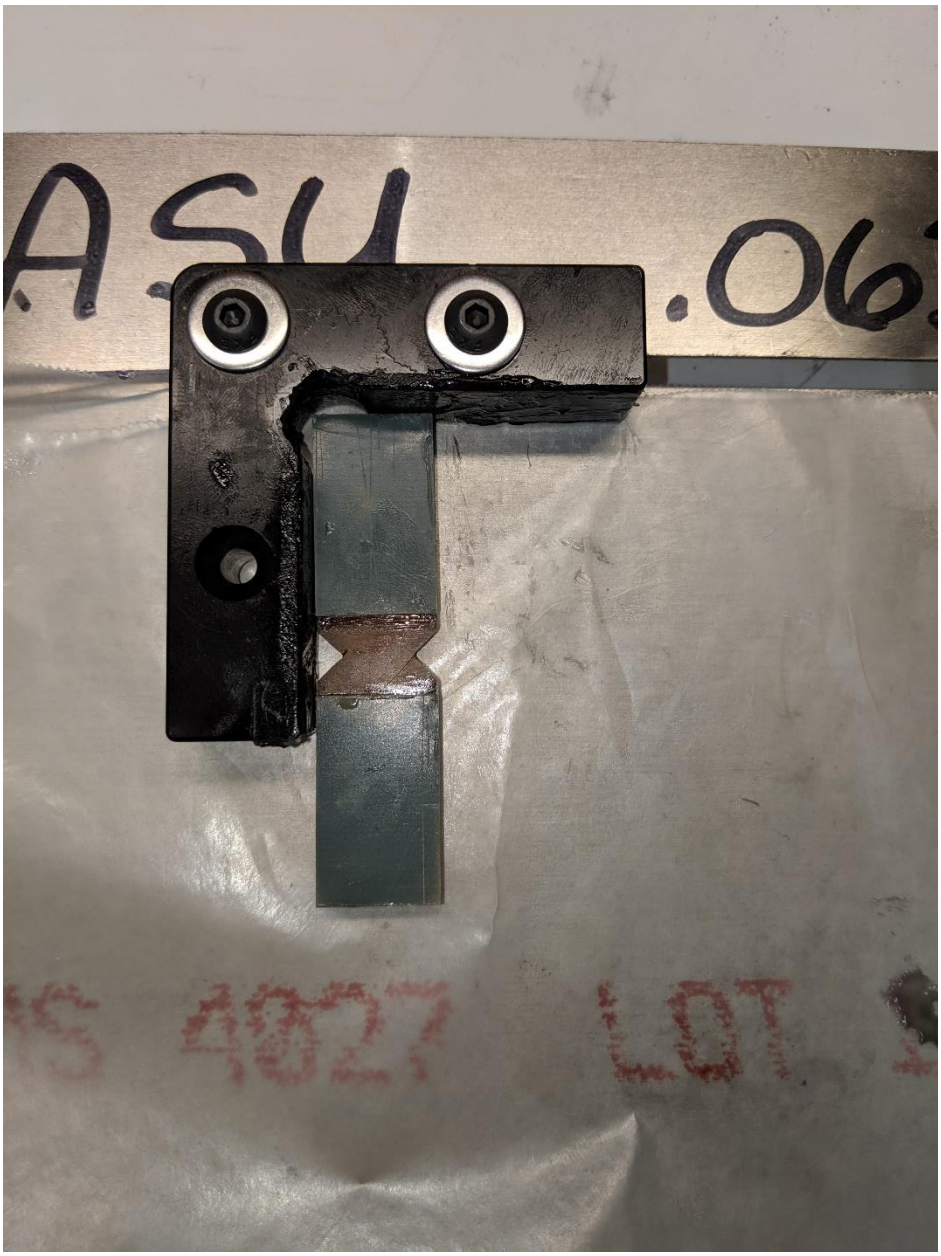

4.19 Alignment Tool for Tabbed Shear Specimens

The black alignment fixture was coated in Dow Corning High Vacuum Grease[6]. Then the specimens were lightly sanded and cleaned on the surfaces to be in contact with the fixture (top and bottom) to ensure the specimens were level and flat and the tabs

[6] https://www.duniway.com/images/_pg/datasheet-DC-150.pdf

would not be loaded in the fixture. The specimens were then painted and speckled as discussed earlier.

Test Machines, Fixtures, Equipment, and Software: Specimens were placed in an Iosipescu Shear fixture[7]. Specimens were first placed in the fixture and then aligned using the built-in alignment tool (Fig. 4.20). The thumb screws on either side were tightened simultaneously until the specimen was sufficiently immobilized.

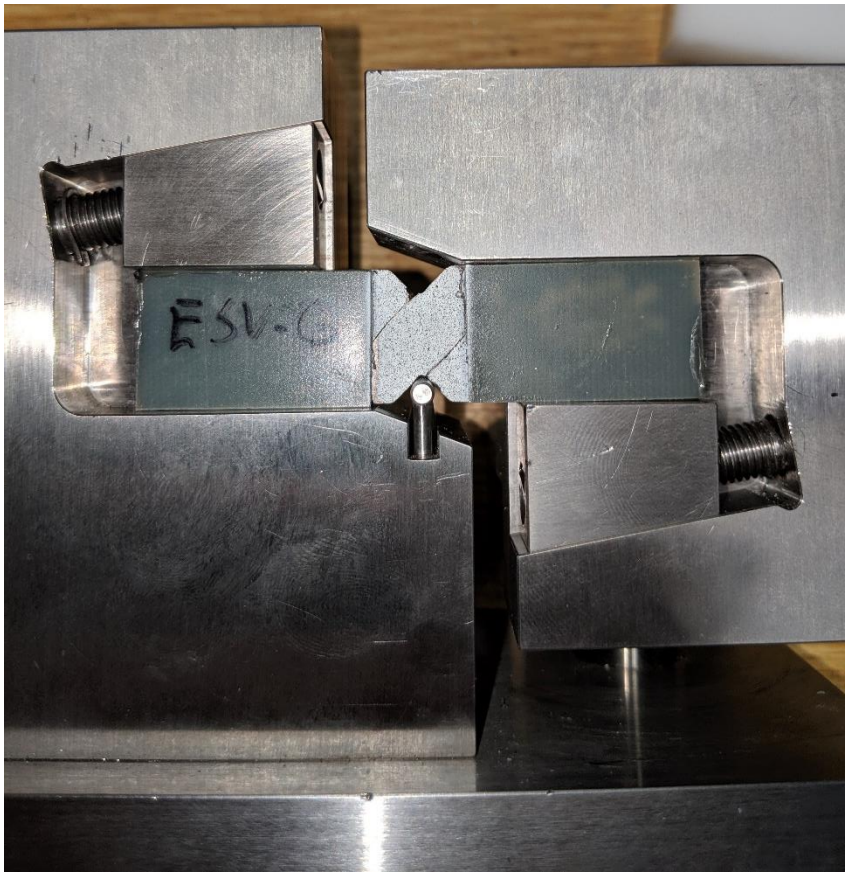

4.20 Tabbed Specimen in Fixture with Alignment Tool Extended

Specimens were loaded in displacement control at a rate of 0.0075 in/min (0.19 mm/min). The test setup can be seen in Fig. 4.21

[7] http://www.wyomingtestfixtures.com/Products/a1.html

4.21 Typical Test Setup for Iosipescu Shear Test

Specimen Photographs: The specimen photographs before the tests are shown in Fig. 4.22 and Fig. 4.23 shows the specimens after testing.

(a)

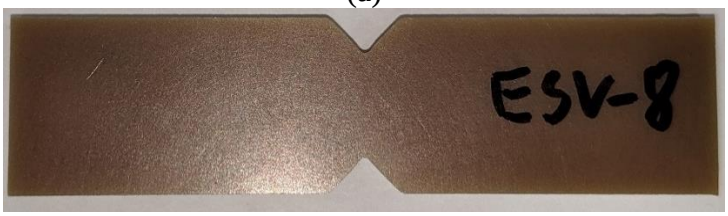

(b)

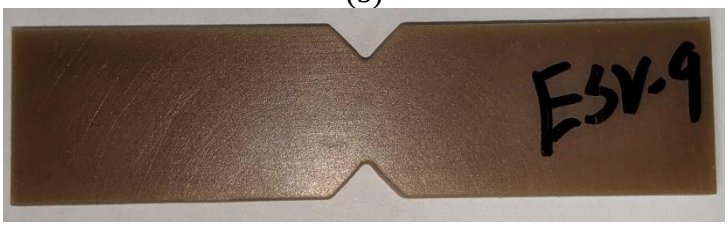

(c)

4.22 (a) ESV-6, (b) ESV-8, and (c) ESV-9 Iosipescu Shear Specimens Pretest

(a)

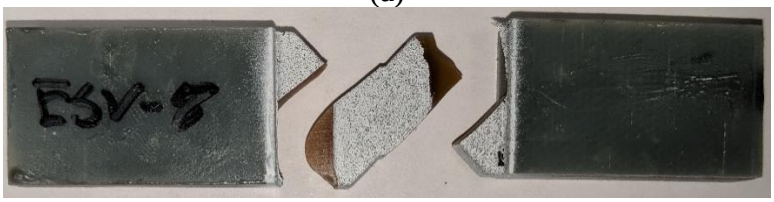

(b)

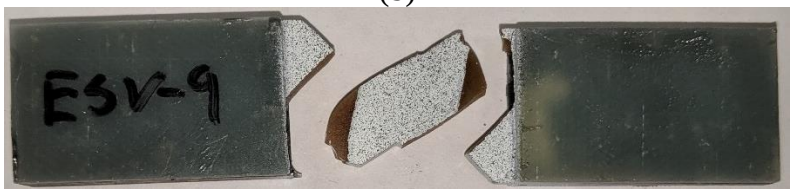

(c)

4.23 (a) ESV-6, (b) ESV-8, and (c) ESV-9 Iosipescu Shear Specimens Posttest

Test Results: Table 4.6 shows a summary of the Iosipescu shear test results.

4.6 Iosipescu Shear Test Results Summary

Replicate	**Loading Rate (in/min)**	**Strain Rate** $\left(s^{-1}\right)$	**G_{12} (psi)**	**Ultimate Strain**	**Peak Stress (psi)**
ESV-6	0.00075	$6(10^{-5})$	145 000	0.0219	5 940
ESV-8	0.00075	$8(10^{-5})$	142 000	0.0250	5 730
ESV-9	0.00075	$7(10^{-5})$	140 000	0.0300	6 690
Average	-	-	142 000	0.0266	5 940
Standard Deviation	-	-	2 210	0.0038	670
Coefficient of Variation	-	-	1.6%	14.3%	11.3%

The strain rate data was obtained from the DIC results and is an average value over the duration of the test. The shear modulus was obtained by taking the linear portion of the stress-strain curve and finding the slope of that line and dividing by two to convert the tensorial shear strain to engineering shear strain.

Fig. 4.24 shows the stress-strain curves for the three replicates.

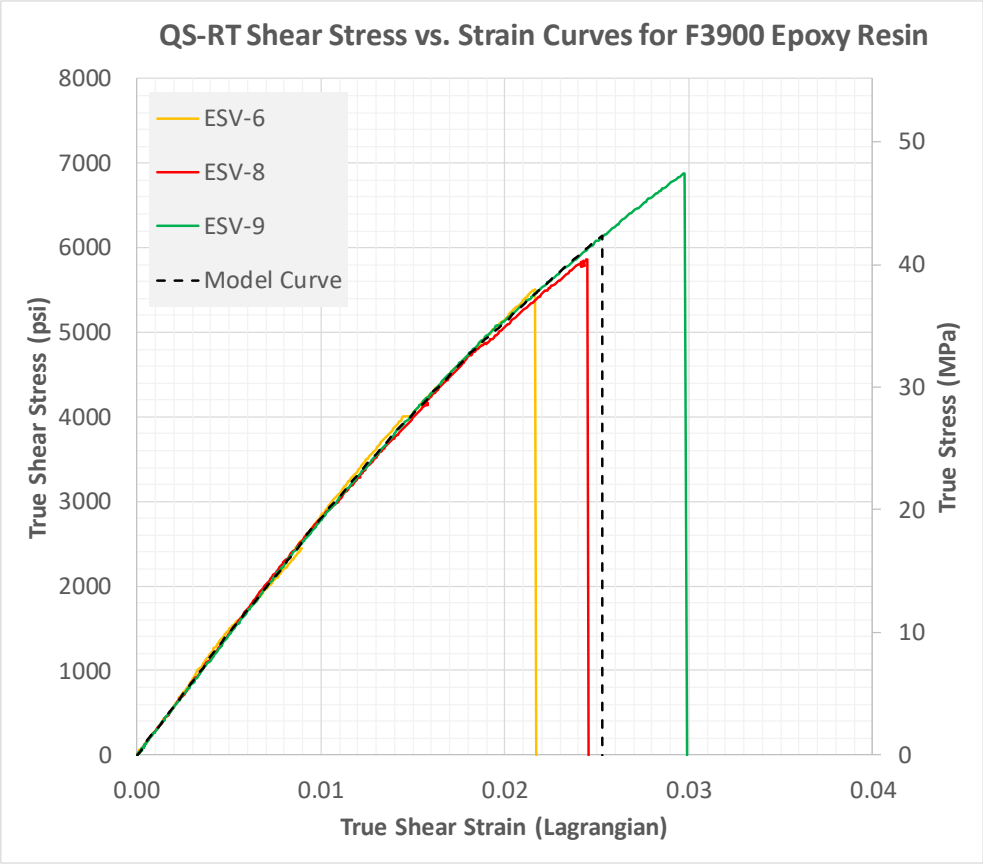

4.24 Shear Stress vs. Tensorial Shear Strain Curves for Iosipescu Shear Tests

Use in Finite Element Model: The Model Curve is used to create the MAT187 card under the input variable LCID_S. This curve is the plastic strain vs. yield stress curve with the plastic strain defined as

$$\varepsilon_{ps} = \varepsilon_s - \frac{\sigma_s}{2G} \tag{5.5}$$

where σ_s is the shear stress at a given point, ε_s defined as the Lagrangian shear strain obtained from DIC, and G is taken as the average shear modulus of the replicates. The curve was then smoothed in a similar fashion as the previous curves. Fig. 4.25 shows the Model Curve.

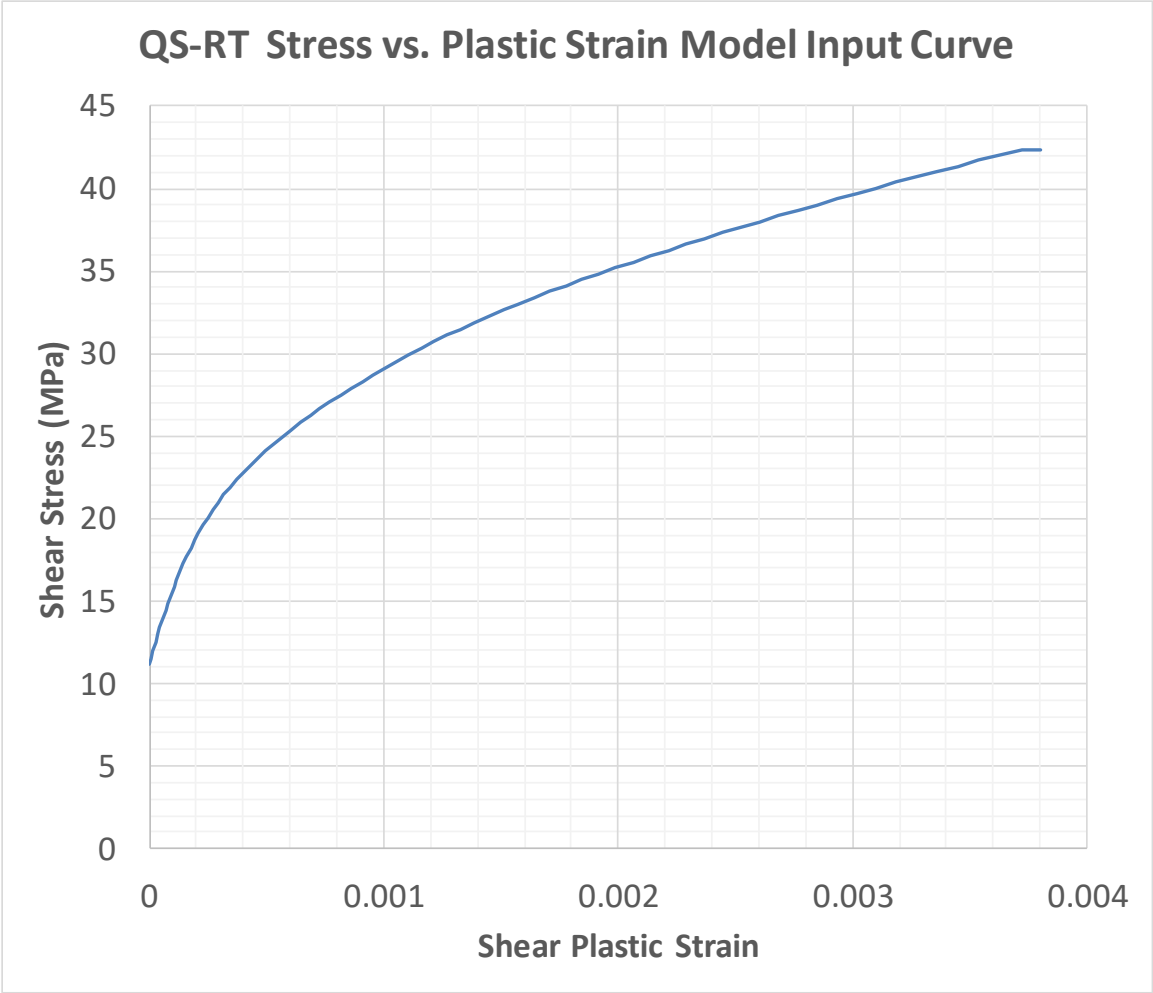

4.25 Model Input Curve for Plastic Shear Strain vs. Shear Stress

4.5 F3900 Matrix Shear Punch Test

Specimen Geometry: Specimens tested follow ASTM D732-17 (2017. A typical specimen is shown in Fig. 4.26.

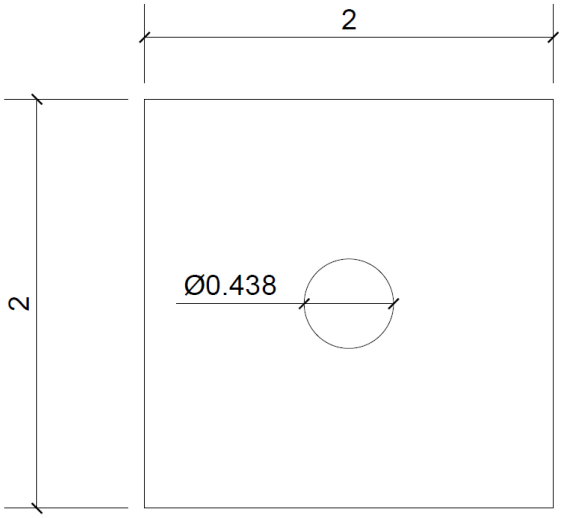

4.26 Shear Punch Test Specimen Geometry with a Thickness of 0.5 (Dimensions in Inches)

The average specimen dimensions in the gage section are shown in Table 4.7.

4.7 Shear Punch Test Specimen Dimensions

Replicate	Punch Width (in)	Specimen Thickness (in)	Cross Sectional Area (in^2)
ESP-1	0.999	0.145	0.455
ESP-2	0.999	0.151	0.474
ESP-3	0.999	0.162	0.509
ESP-4	0.999	0.149	0.467
Average	0.999	0.152	0.476
Std. Dev	0.000	0.007	0.023
Coeff of Var.	0%	4.8%	4.9%

Test Machines, Fixtures, Equipment, and Software: Specimens were placed in a Punch Shear fixture[8] with the large washers on top (Fig. 4.27). The four corner bolts were screwed into place (Fig. 4.28). The fixture was then screwed into the test frame using a threaded adapter (Fig. 4.29). Specimens were loaded in displacement control at a rate of 0.005 in/min.

4.27 Specimen Placed on Punch Tool

[8] http://www.wyomingtestfixtures.com/Products/a6.html

4.28 Punch Shear Fixture with Specimen

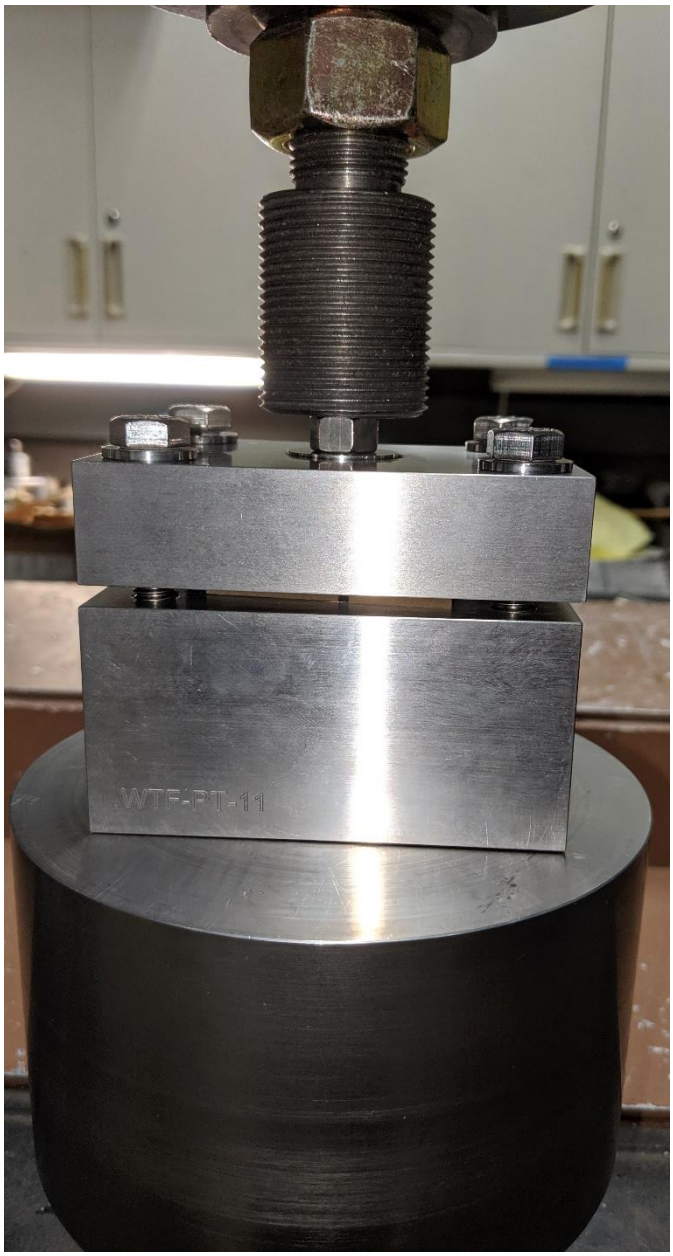

4.29 Shear Punch Fixture and Threaded Adapter

Test Data Reduction: The load vs. displacement data was obtained from the output of the load frame. The peak load was divided by the sheared area found in Table 4.7 to give the peak shear stress. Fig. 4.30 shows the load vs displacement curves for the four specimens.

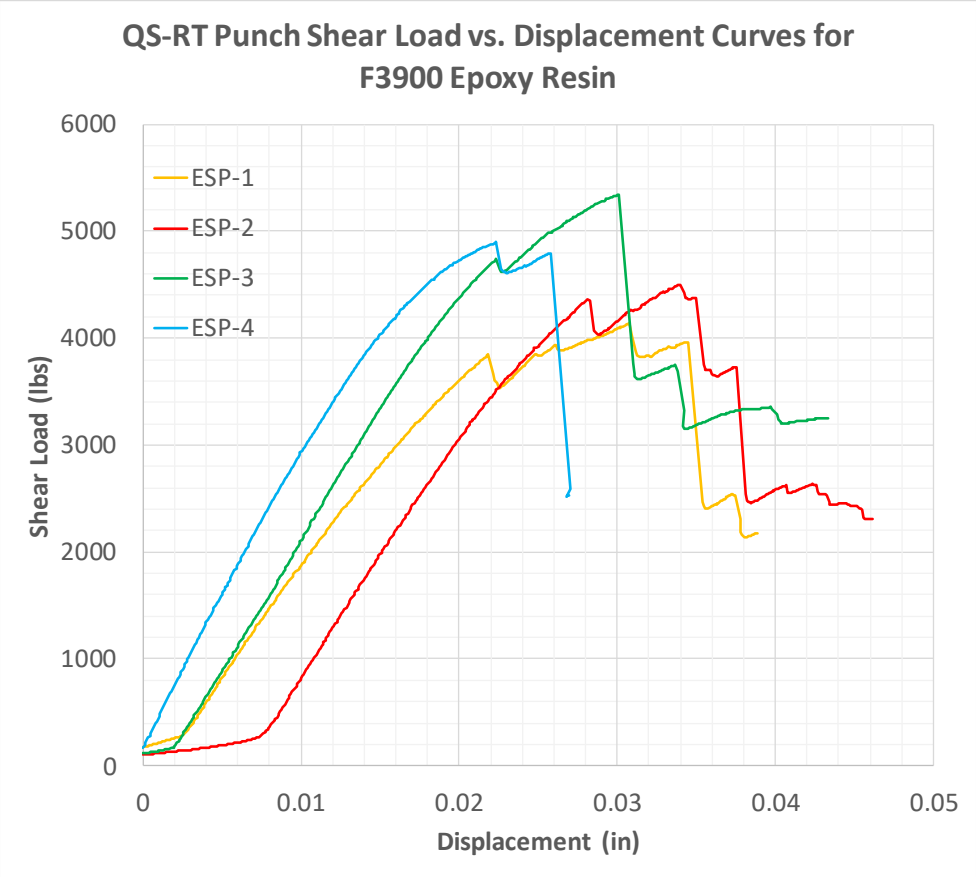

4.30 Shear Punch Load vs. Displacement Curves

Specimen Photographs: The specimen photographs before the tests are shown in Fig. 4.31 and Fig. 4.32 shows the specimens after testing.

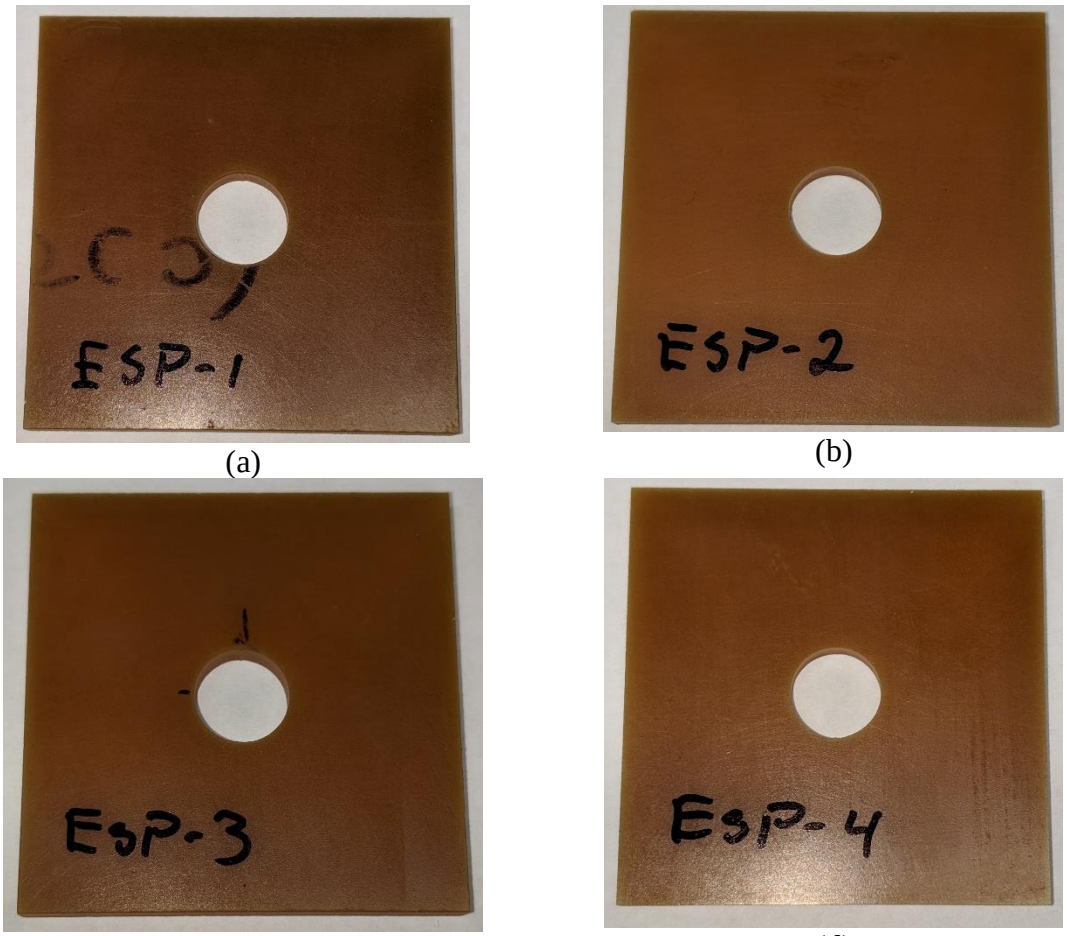

(a) (b) (c) (d)

4.31 (a) ESP-1, (b) ESP-2, (c) ESP-3, and (d) ESP-4 F3900 Epoxy Shear Punch Specimens Pretest

(a)

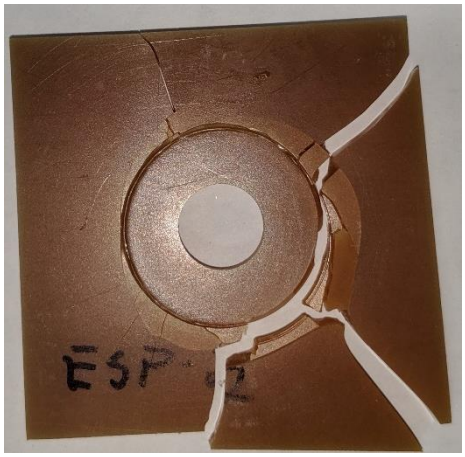

(b)

(c)

(d)

4.32 (a) ESP-1, (b) ESP-2, (c) ESP-3, and (d) ESP-4 F3900 Epoxy Shear Punch Specimens Posttest

Test Results: Test results for the four specimens are shown in Table 4.8.

4.8 Punch Shear Test Results Summary

Replicate	**Loading Rate (in/min)**	**Peak Stress (psi)**
ESP-1	0.005	9 090
ESP-2	0.005	9 490
ESP-3	0.005	10 500
ESP-4	0.005	10 476
Average	-	9 890
Standard Deviation	-	712
Coefficient of Variation	-	7.2%

Compared to the Isopescu shear test, the punch shear shows about a 3000 psi increase (~50%) in the peak stress which is similar to the results reported by Liu and Piggott (1995) for their epoxy tests at room temperature. While their difference in strengths is smaller than the values reported in this study, their data also shows a larger range in shear values. The failure patterns and force vs. displacement graphs also match the results of the F3900 matrix tests.

4.6 Experimental Observations.

The overall failure of the tension and Isopescu shear tests were very rapid and faster than the framerate of the DIC so no analysis on the onset of failure and its propagation can be done though correlations with the failure patterns visually were made. Tension tests failed almost entirely in the gage section with ET-7 (figure 4.4(d)) being the only specimen to fail near the geometry change. The failure also showed a slight plastic deformation before failing in a brittle fashion causing the material to lose its load carrying capacity suddenly. The Isopescu shear test failed along two diagonal lines originating from the fixture in the top right and bottom left corners. Again, like the

tension test, the failure was brittle with a slight plastic deformation before the specimen failed.

The compression specimens failed much more gradually with an initial lateral deformation occurring which then resulted in the material cracking and the front and back material breaking off. The stress cracks can be seen in figure 4.13 which also shows the high lateral deformation of the material. The barreling out of the specimen occurred between 0.15 and 0.25 strain while the cracking of the specimen occurred around 0.35 strain.

The shear punch test specimens failed incrementally in stages as the material cracked and failed until, ultimately, the peak load was found and the test was stopped. The failure pictures (figure 4.32) show this cracking behavior and from the force vs. displacement graph the incremental nature of the failure can be seen with slight reloading of the material happening after each drop in force.

5. T800s Fiber Experimental Test Details and Results

5.1 Overview

The details of the T800s fiber test setup and analysis are found in this section. The test was done in accordance with ASTM C1557 and any deviations from this standard are noted.

5.2 T800s Fiber Tension Test

Specimen Geometry: Specimens were assumed to be single fiber specimens with an original gage length of 2" that is fixed at either end. The fibers were assumed to have a consistent diameter of approximately 5.66 μm. This was estimated by massing a known length of fiber and assuming the cross-sectional area was a circle.

Specimen Preparation: Specimens were prepped by creating a specimen guide shown in figure 5.1.

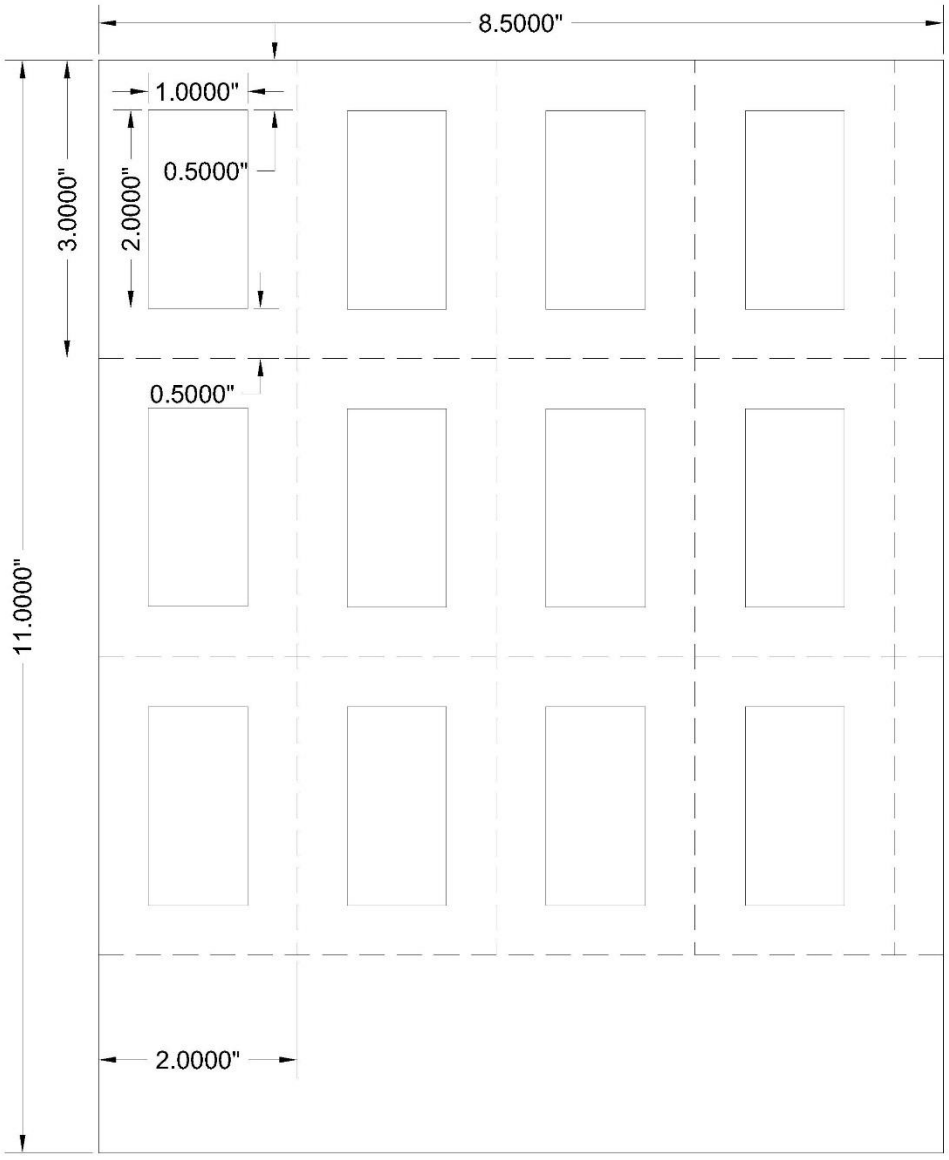

5.1 Typical Template Layout.

Individual lengths of yarn, about 12 in. in length, were cut from the spool (figure 5.2) of yarn that was obtained from Toray.

5.2 Full Spool of T800s Yarn

The template was then printed off and measured to ensure that the aspect ratio of the paper was correct and all gage lengths were 2 in. The midpoint of every gage section was then marked with a pencil to help guide where the fibers were to be placed. Slits were cut in the middle of the gage section (denoted by the solid black line) at a length of approximately 0.5 in parallel to the shorter ends of the individual specimen. From there an individual fiber was manually removed from the yarn taking care to not damage the fiber and trying to ensure that only one fiber was removed. The fiber was laid across the gage section parallel to the long edges and so that the fiber laid directly in the previously made marks (figure 5.3).

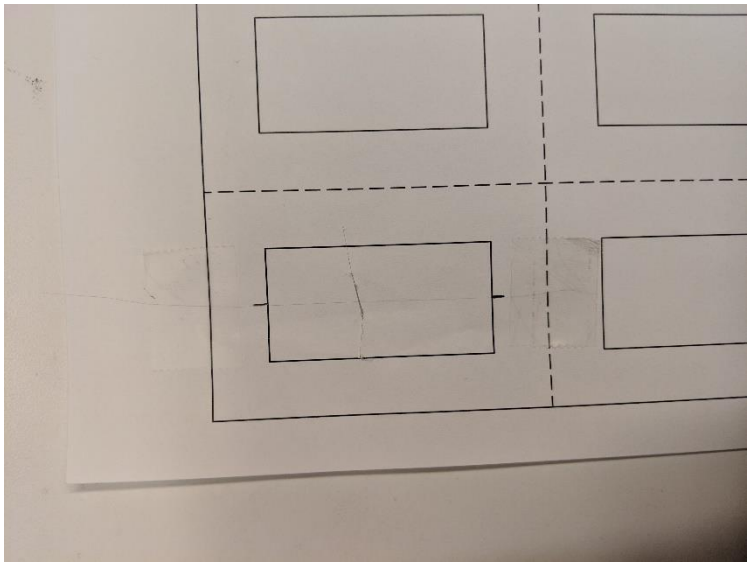

5.3 Fiber Adhered to Paper with Tape Only

Tape was then used to hold the fiber to the page but placed about 1/8 in. away from the solid black line. Elmer's White Glue was then used to adhere the fiber to the paper by placing a small dab of glue such that the edge of the glue touched by did not overlap the solid black line (figure 5.4). The glue was then allowed to dry for approximately two hours or until the glue became translucent.

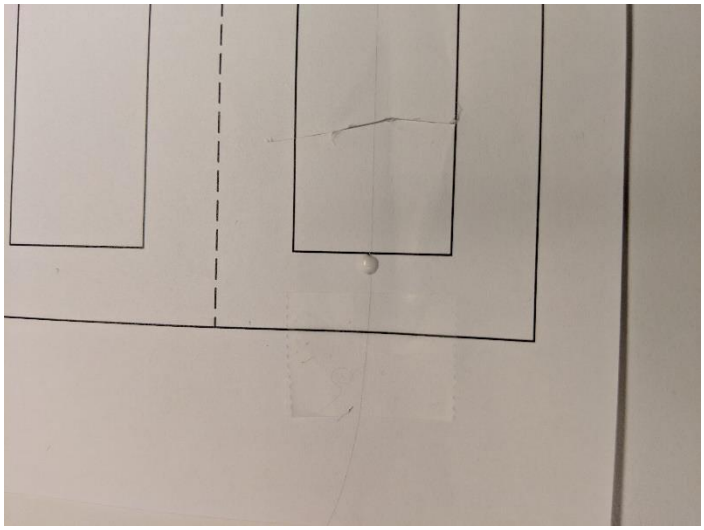

5.4 White Glue Placed, but Not Dried, on Fiber

Test Machines, Fixtures, Equipment, and Software: Specimens were loaded on a low force test frame from Accudek (model number: ART310-G54) in displacement control. Specimens were loaded at a rate of 0.01 in/min specified in the Ensemble software version:4.09.002.0005. The load was captured using a 1 lb load cell from Interface model number WMCP-500G. The displacements were captured using an external LVDT (Novotechnik TR-0050) leveled and squared with the actuator. All loads and displacements were captured in a labview environment (software version:15.0f2).

Specimens were affixed to the load frame using a hand clamp on the actuator side and a rigid clip on the load cell side that was affixed to the load cell using a standoff screw. The clamping was done outside the gage section so the fibers would not be potentially damaged prior to testing. Once the specimens were in place the edges of the paper were cut so the only material being loaded in the frame was the T800 fiber. A top down view of the test setup can be seen in figure 5.5 and a side view of the setup can be seen in figure 5.6.

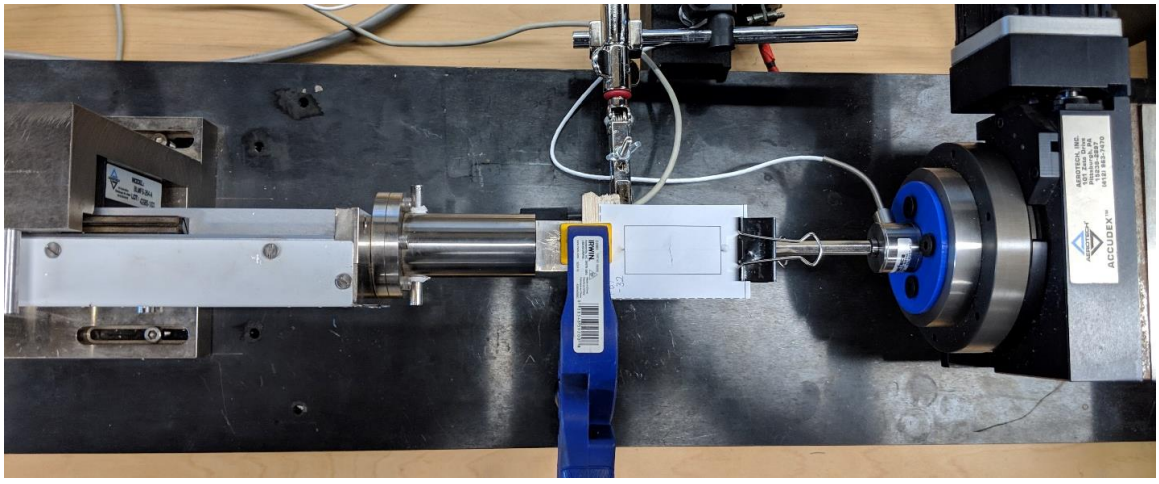

5.5 Top-Down View of Tension Test Setup for T800s Fiber

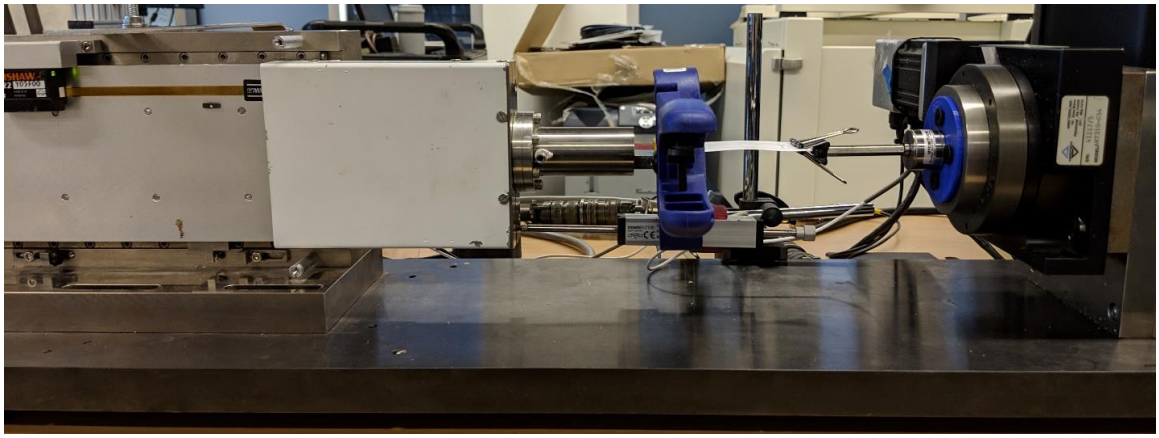

5.6 Side View of Tension Test Setup for T800s Fiber

Specimen Photographs: Figure 5.7 shows the specimens before testing and figure 5.8 shows the specimens after testing.

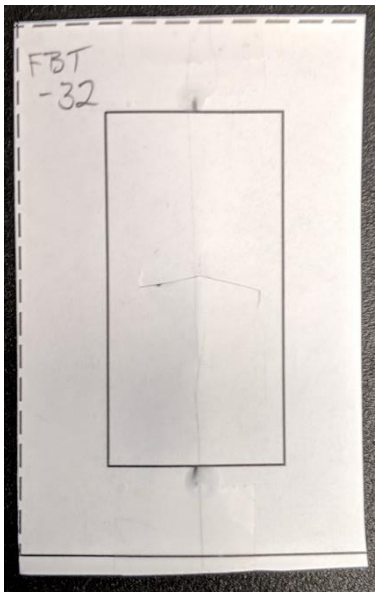

(a)

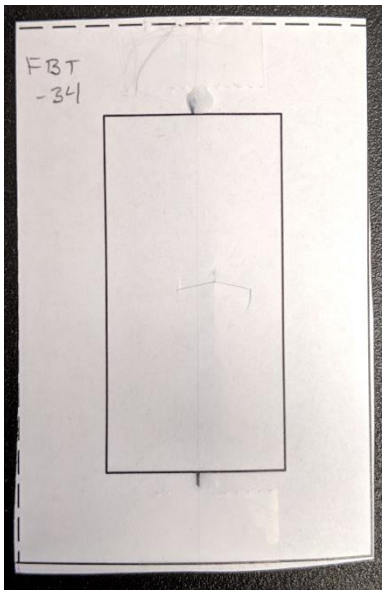

(b)

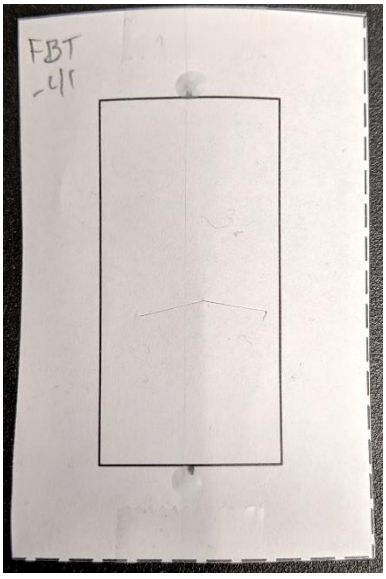

(c)

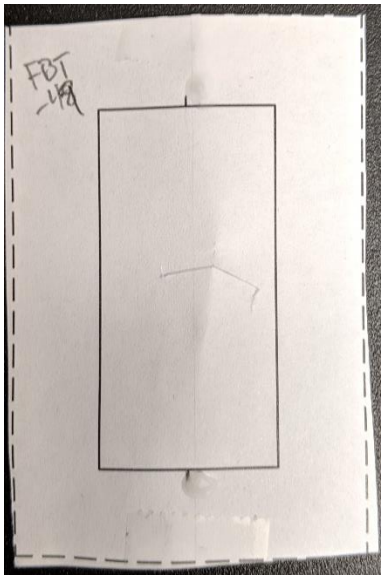

(d)

5.7 FBT-32 (a), FBT-34 (b), FBT-41 (c), FBT-49 (d), EC-8 (e) T800s Fiber Tension Specimens Pretest

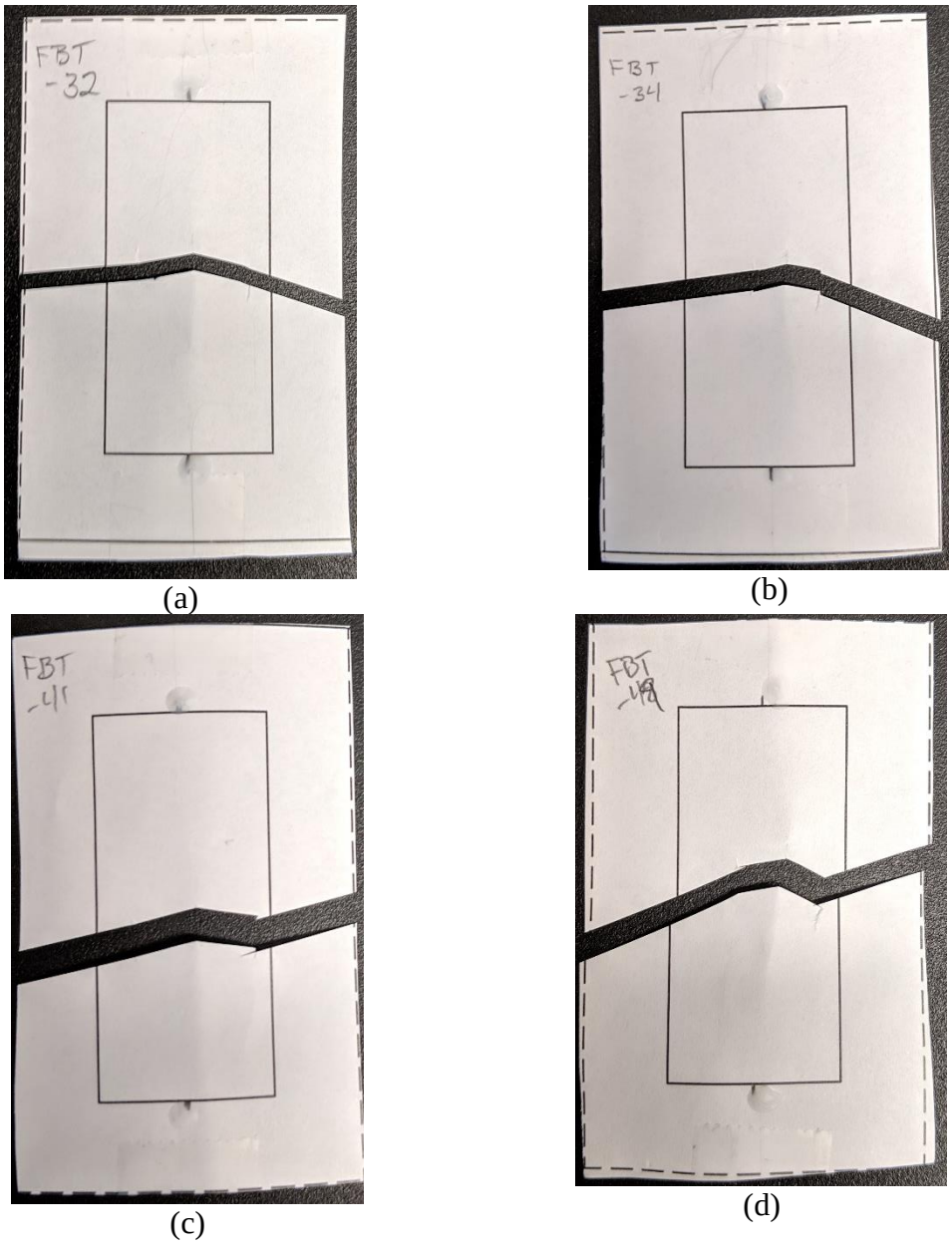

(a) (b) (c) (d)

5.8 FBT-32 (a), FBT-34 (b), FBT-41 (c), and FBT-49 (d) T800s Fiber Tension Specimens Posttest

Test Results: Table 5.1 shows the results from the tension tests for the fiber specimens. Any specimens where there was succ. Specimens 32, 34, 41, and 49 were chosen because they exhibited the most consistent failure with a single peak. Multiple peaks during loading suggests that multiple fibers were being loaded at once which

would skew the results of the test. Figure 5.9 shows the individual engineering stress vs. engineering strain curves for the four replicates.

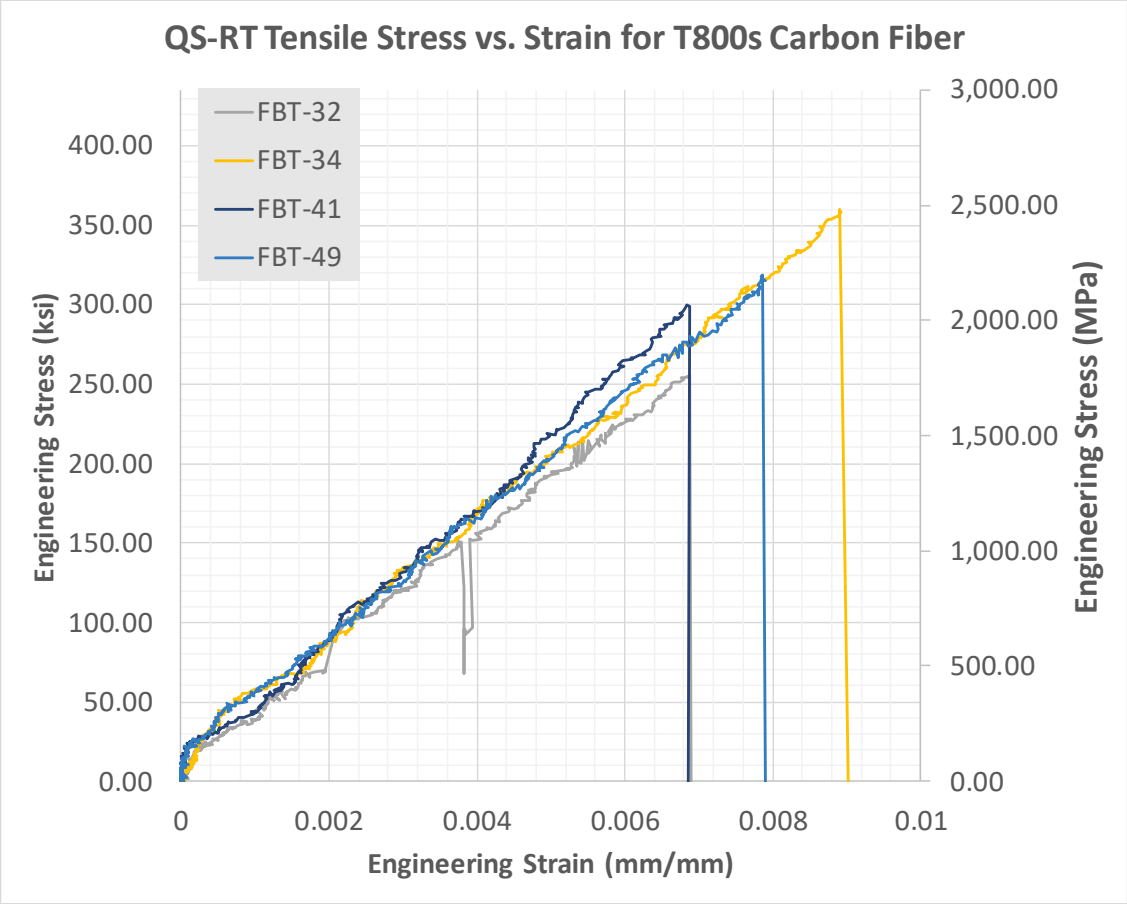

5.9 Stress vs. Strain Curve for T800s Carbon Fiber

5.1 T800 Fiber Tension Test Results Summary

Replicate	**Loading Rate (in/min)**	**E_{22} (Msi)**	**Ultimate Strain**	**Peak Stress (ksi)**
FBT-32	0.01	37.92	0.0069	255.7
FBT-34	0.01	40.28	0.0089	360.0
FBT-41	0.01	43.17	0.0069	299.8
FBT-49	0.01	40.63	0.0079	318.8
Average	-	40.5	0.0076	308.6
Standard Deviation	-	2.15	0.00097	43.25
Coefficient of Variation	-	5.3%	12.7%	14%

The variability in the ultimate strain and peak stress values suggests that the fibers could be prone to imperfections in the individual fibers which would cause certain lengths of fibers to fail at different points. Therefore a statistical distribution of strengths of the fibers would be necessary to capture the full behavior of the material. This could also introduce a size effect where the length of fiber has an impact on the overall strength of the material.

6. LS-DYNA Simulation of F3900 Matrix Verification Tests Using MAT187

6.1 LS-DYNA Simulation Overview

This section serves as a summary of the simulations conducted to verify the deformation and failure material models used for the F3900 Matrix. The material model selected is MAT187: Semi-Analytical Model for Polymers. This model was chosen for its allowance of tension, compression, and shear stress-strain curves to be input separately and allows for the deformation of the material to be specified in each of the directions. Similar material models used for plastic behavior such as MAT089: Plasticity Polymer and MAT003: Plastic Kinematic assume the shape of the stress-strain behavior based on material constants but do not distinguish between tension, compression, or shear.

A series of three tests were used to verify the inputs for the material model as well as the failure criteria. These were both single element and multi-element tension, compression, and shear tests.

The simulations were then compared against their respective experimental model curves to verify that the material model was outputting the expected results and that all inputs were correct. The stresses and strains from the experiment were taken at similar points to the experimental data when processing the multi-element simulations. The data was also taken at the surface of the model and over the area used in the post processing of the data.

6.2 LS-DYNA MAT187 Theory Overview

The F3900 Matrix material model that was used for all simulations is MAT187 – Semi-Analytical Model for Polymers (SAMP). This model was developed by Kolling, et Al (2005) to allow for a tabulated plasticity model in tension, compression, and shear with an option to include data at various strain rates. The stress-strain curves used as input are converted to plastic-strain vs. stress space which then allows for the material model to solve for the yield surface coefficients based on a generalized quadratic formulation:

$$f = \boldsymbol{\sigma}^{\mathbf{T}}\mathbf{F}\boldsymbol{\sigma} + \mathbf{B}\boldsymbol{\sigma} + F_0 \tag{7.1}$$

where

$$\boldsymbol{\sigma} = \begin{pmatrix} \sigma_{xx} \\ \sigma_{yy} \\ \sigma_{zz} \\ \sigma_{xy} \\ \sigma_{yz} \\ \sigma_{zx} \end{pmatrix} \quad \mathbf{F} = \begin{pmatrix} F_{11} & F_{12} & F_{12} & 0 & 0 & 0 \\ F_{12} & F_{11} & F_{12} & 0 & 0 & 0 \\ F_{12} & F_{12} & F_{11} & 0 & 0 & 0 \\ 0 & 0 & 0 & F_{44} & 0 & 0 \\ 0 & 0 & 0 & 0 & F_{44} & 0 \\ 0 & 0 & 0 & 0 & 0 & F_{44} \end{pmatrix} \quad \mathbf{B} = \begin{pmatrix} F_1 & 0 & 0 & 0 & 0 & 0 \\ 0 & F_1 & 0 & 0 & 0 & 0 \\ 0 & 0 & F_1 & 0 & 0 & 0 \\ 0 & 0 & 0 & 0 & 0 & 0 \\ 0 & 0 & 0 & 0 & 0 & 0 \\ 0 & 0 & 0 & 0 & 0 & 0 \end{pmatrix} \tag{7.2}$$

This can then be reformulated in terms of the first two stress invariants, defined:

$$\begin{aligned} p &= -\frac{\sigma_{xx} + \sigma_{yy} + \sigma_{zz}}{3} \\ \sigma_{vm} &= \sqrt{\frac{3}{2}\left(\left(\sigma_{xx} + p\right)^2 + \left(\sigma_{yy} + p\right)^2 + \left(\sigma_{zz} + p\right)^2 + 2\left(\sigma_{xy}^2 + \sigma_{yz}^2 + \sigma_{zx}^2\right)\right)} \end{aligned} \tag{7.3}$$

The generalized quadratic formulation is then rewritten as:

$$f = \sigma_{vm}^2 - A_0 - A_1 p - A_2 p^2 \le 0 \tag{7.4}$$

where

$$A_0 = -F_0 \ , \ A_1 = 3F_1 \ , \ and \ A_2 = 9\left(1 - F_{11}\right) \tag{7.5}$$

Which can then be used to define the other coefficients resulting in

$$F_0 = -A_0 \ , \ F_1 = \frac{A_1}{3} \ , \ F_{11} = 1 - \frac{A_2}{9} \ , \ F_{44} = 3 \ , \ and \ \ F_{12} = F_{11} - \frac{F_{44}}{2} = -\left(\frac{1}{2} + \frac{A_2}{9} \right) \quad (7.6)$$

The coefficients can then be computed from three different tests: uniaxial tension, uniaxial compression, and simple shear by using the various yield stresses which takes the form:

$$\begin{aligned} A_0 &= 3\sigma_s^2 \\ A_1 &= 9\sigma_s^2 \left(\frac{\sigma_c - \sigma_t}{\sigma_c \sigma_t} \right) \\ A_2 &= 9 \left(\frac{\sigma_c \sigma_t - 3\sigma_s^2}{\sigma_c \sigma_t} \right) \end{aligned} \quad (7.7)$$

Or alternatively these can be defined relating to the formulation in stress space:

$$\begin{aligned} F_1 &= F_0 \left(\frac{1}{\sigma_c} - \frac{1}{\sigma_t} \right) \\ F_{11} &= -\frac{F_0}{\sigma_c \sigma_t} \\ F_{44} &= -\frac{F_0}{\sigma_s^2} \end{aligned} \quad (7.8)$$

In order to ensure the yield surface would be convex, all eigenvalues of the **F** coefficient matrix must be non-negative this leads to following relationships between the various coefficients:

$$\left. \begin{matrix} F_{11} + 2F_{12} \geq 0 \\ F_{11} - F_{12} \geq 0 \\ F_{44} \geq 0 \end{matrix} \right\} \Rightarrow \begin{cases} 3\sigma_s^2 \geq \sigma_t \sigma_c \\ -F_0 \geq 0 \end{cases} \quad (7.9)$$

Based on the input the program then picks the yield surface shape based on the amount of load input curves given to the program. This is done because the only required

stress-strain curve is the tension curve. If this is the case then the program assumes that the yield surface behaves like a von Misses cylinder and $\sigma_c = \sigma_t$ and $\sigma_s = \sigma_t / \sqrt{3}$. The yield surface in this case is not specifically convex. When exactly two load curves have been defined the yield surface is assumed to behave like a Drucker-Prager cone and the other two stress curves are defined based on the two input curves. If all three curves are defined in the input, then yield surface is assumed to be convex and quadratic in the invariant plane. If the yield surface is not convex based on the input by the user, there is an option to scale the shear yield stress until a convex solution is reached. When all four input curves are defined the yield surface becomes overly specified and, in conjunction with the RBCFAC input variable, becomes a piece-wise equation based on the various yield stress values. This takes the shape show in figure 6.1.

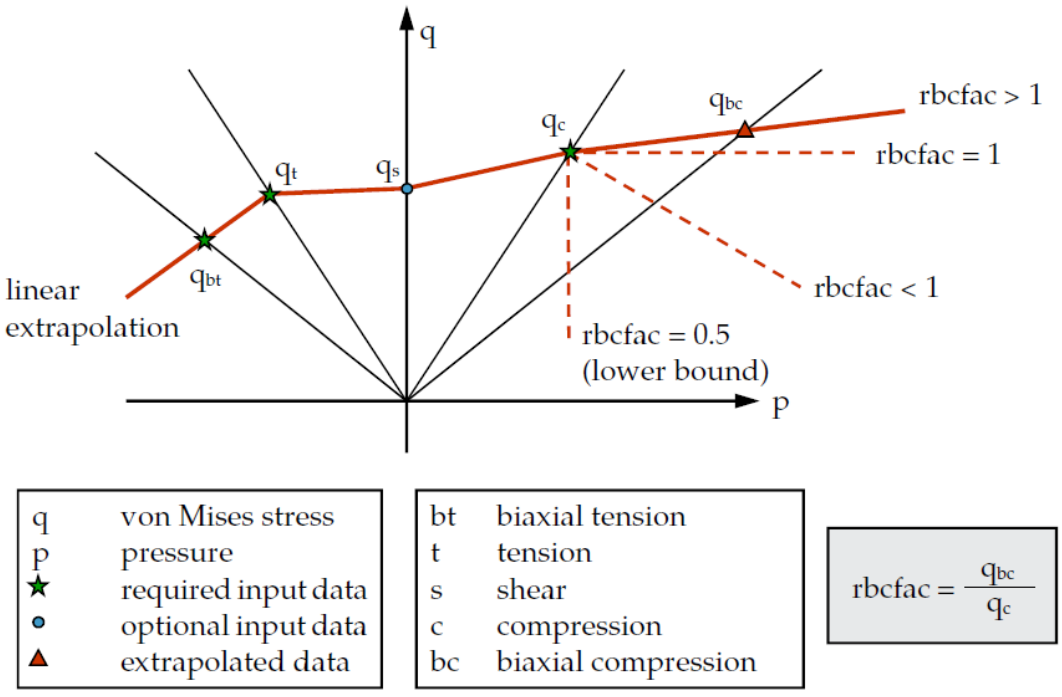

6.1 Piece-wise Yield Surface Used in SAMP

During this study it was found that the most stable and consistent with the experimental results were found when all three curves were used as input: tension compression and shear, and the biaxial curve was input was generated using the tension experiment data scaled by 80%. The RBCFAC was calibrated based on the compression multi-element simulation as it was the only simulation where the results were dependent on this variable. All other multi-element simulations were unaffected.

The failure, similar to the deformation, allows for asymmetry between the compression, tension, and shear with the main variable being the effective plastic strain at failure. From there the asymmetry in the different loading directions is handled by a scale factor that is a function of the triaxiality of the element. This is done using a tabulated generalization of the Johnson-Cook criterion as discussed in Dubois et al (2006). The equivalent plastic failure strain then takes the form of the following equation:

$$\varepsilon_{pf} = D_c\left(\dot{\varepsilon}_p\right) LCID\_TRI\left(\frac{p}{\sigma_{vm}}\right) \tag{7.10}$$

Where D_c is a function of the plastic strain rate and as discussed LCID_TRI is the tabulated scale factor that is a function of the triaxiality of the element.

6.3 General Modeling Techniques

The goal of all the multi-element simulations was to replicate the experiment test conditions as accurately as possible while reducing the computational effort of the model. Where possible the symmetry of the model was leveraged in order to reduce the number of elements. This was achieved in the compression simulation across all three principal axes, in the tension simulation this was achieved vertically and through the thickness of the specimen, and in the shear simulation this was achieved only through the thickness of

the elements. Figures 6.2 through 6.4 show an isometric view of the multi-element models.

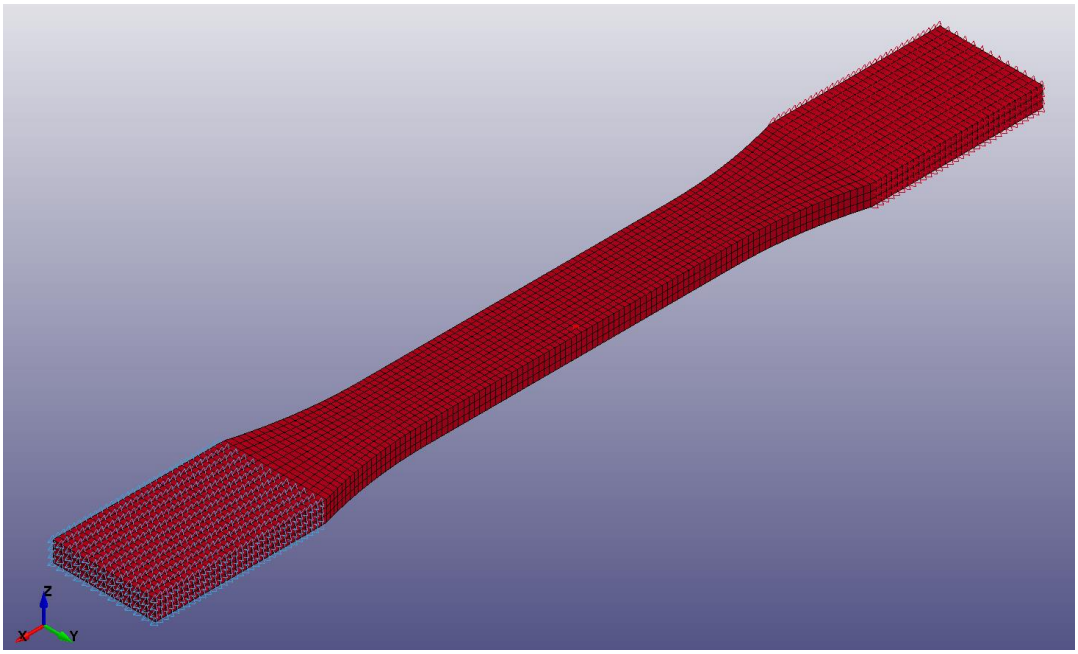

6.2 Tension Multi-Element Verification Model Isometric View

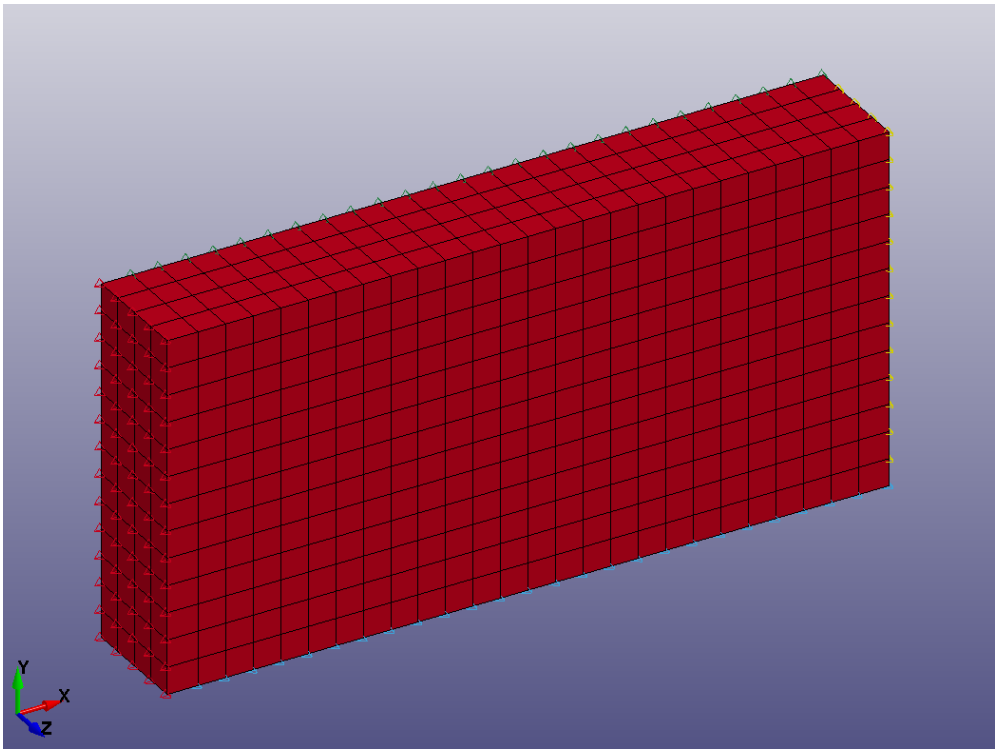

6.3 Compression Multi-Element Verification Model Isometric View

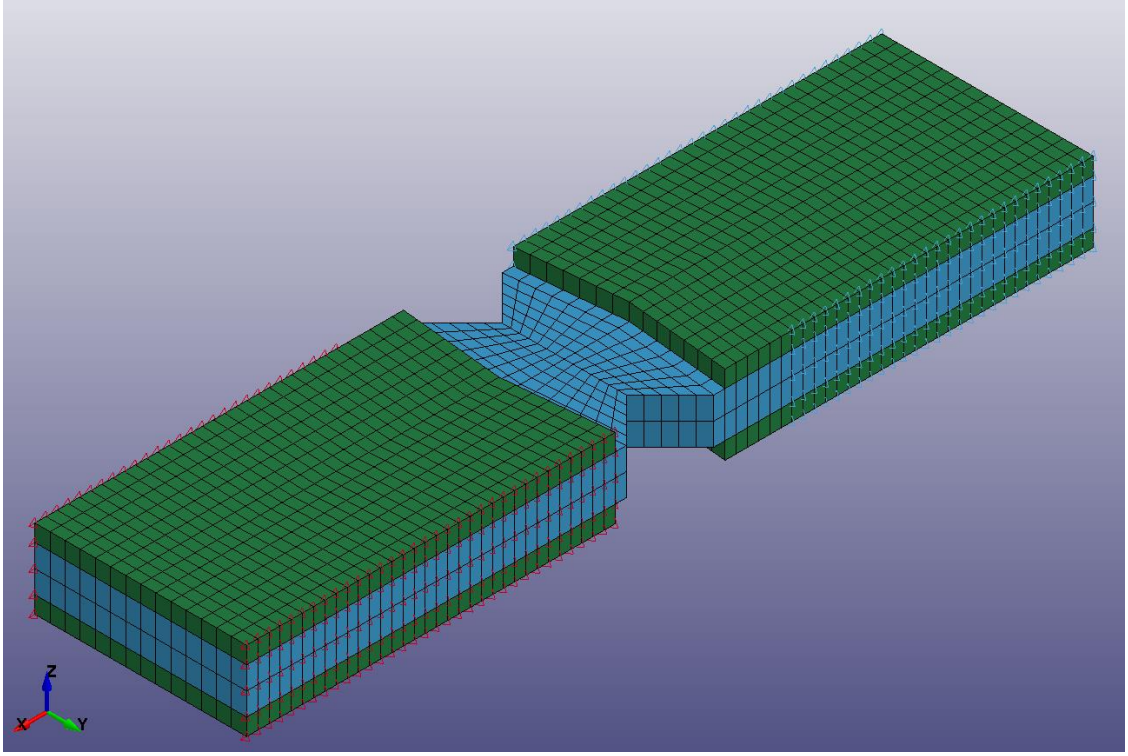

6.4 Shear Multi-Element Verification Model Isometric View

The typical strain rate was increased from the experimental strain rates to reduce computational effort. Since the experiments lasted between 400 and 800 seconds this would cause the computer clock time to be unreasonable. The simulation strain rate is then increased by a factor of 100 to 1000 (down to between 0.4 and 4 seconds) while ensuring that all energies are close to zero except the internal energy. Figure 6.5 shows a typical plot of the energies including: total, internal, and kinetic. From the plot the total and internal energies are almost the same with the kinetic energy close to or equal to zero.

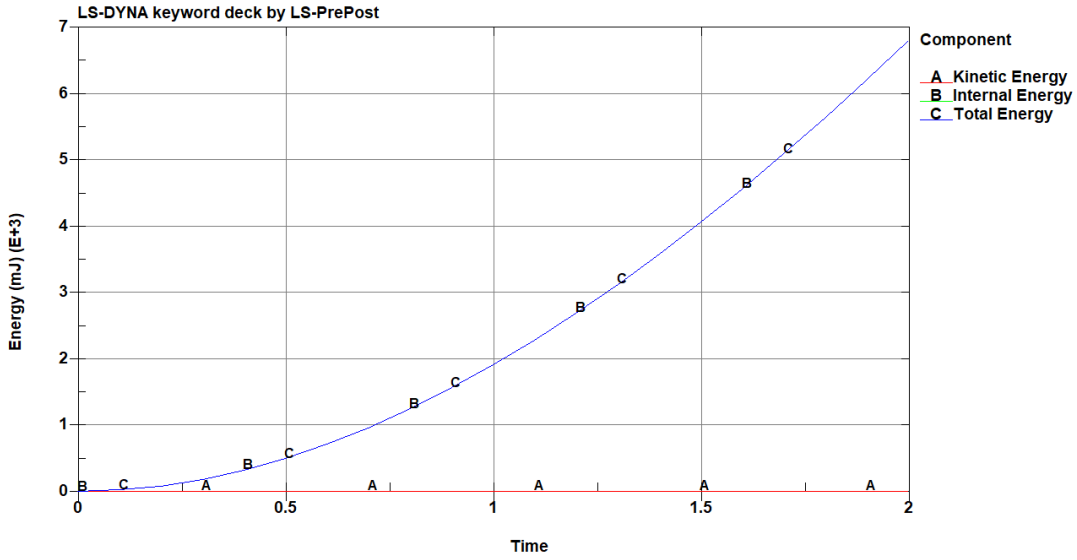

6.5 Typical Energy Plot

When modeling the failure of the F3900 matrix the LCID_TRI and EPFAIL model variables were utilized where EPFAIL was set to 0.00719 which was the plastic strain at failure for the tension test and the LCID_TRI variables were calibrated so the single element tests failed at the appropriate strain and stress values. This curve is shown in Table 6.1.

6.1 Failure Model Input Curve

Triaxiality	**Scale Factor**
-0.333	1.00
0.000	0.78
0.333	48.565

6.4 LS-DYNA Simulation of F3900 Matrix Single Element

6.4.1 Simulation Modeling

All three single element tests were run in the same model using the same material card. The three elements were all loaded in displacement control with the boundary conditions shown in figures 6.6 through 6.8. When comparing the other stress

components to the stress desired all were numerically equal to zero. The pressure vs. von mises curve was generated for the shear elements in order to ensure a state of pure shear was achieved and that the simulation results were valid. Elements were loaded passed the end point for all experimental curves to ensure the entire experimental curve was being measured against. This was done in both the deformation and failure simulations.

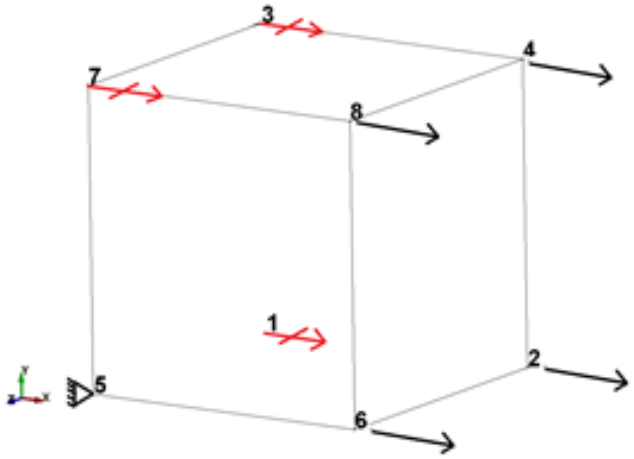

6.6 Tension Single Element Loading and Boundary Conditions

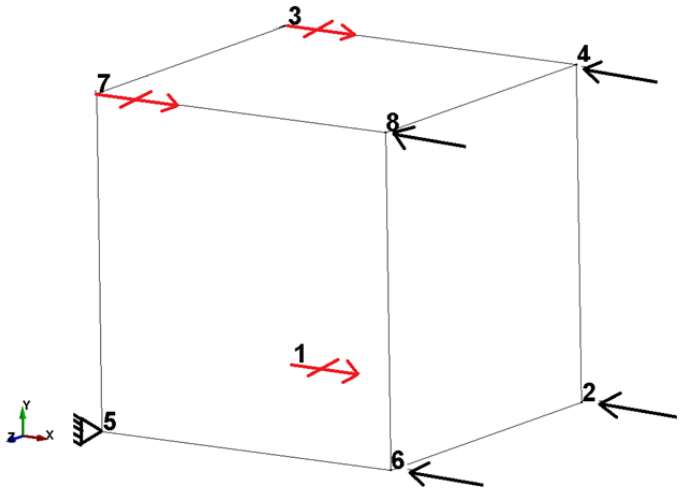

6.7 Compression Single Element Loading and Boundary Conditions

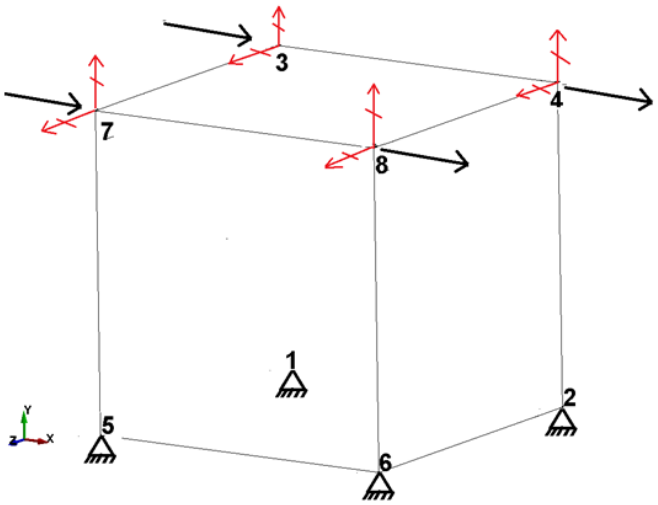

6.8 Shear Single Element Loading and Boundary Conditions

6.4.2 Results

Figure 6.9 shows the longitudinal stress vs. strain curve for the tension single element with deformation only.

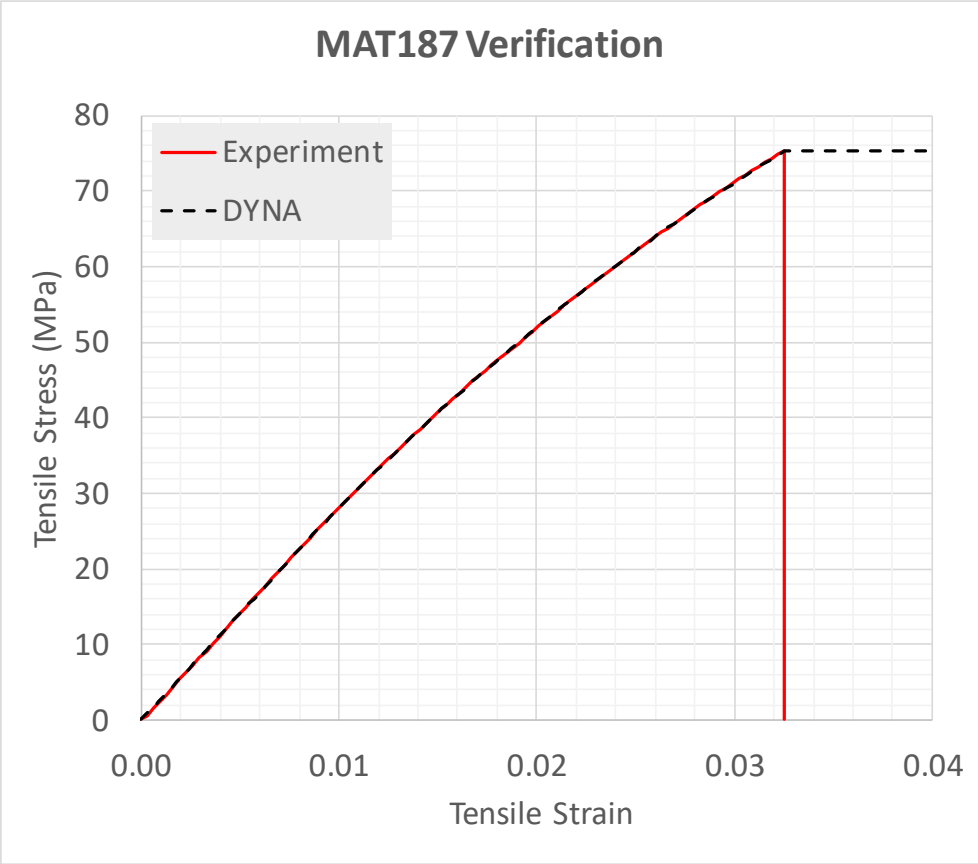

6.9 Tension Single-Element Stress vs. Strain Plot for Deformation Only

Figure 6.10 shows the longitudinal stress vs. strain curve for the tension single element with deformation and failure.

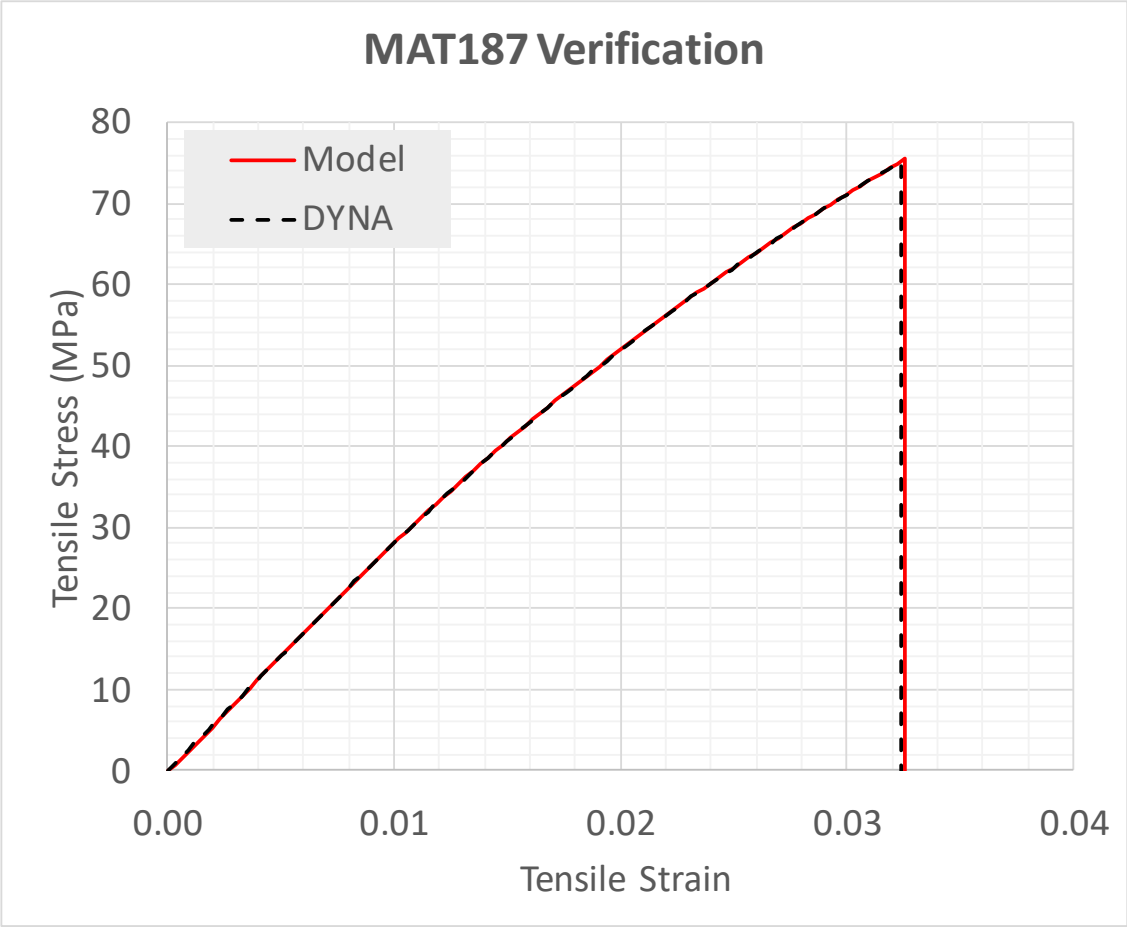

6.10 Tension Single-Element Stress vs. Strain Plot for Deformation and Failure

Figure 6.11 shows the longitudinal stress vs. strain curve for the compression single element with deformation only.

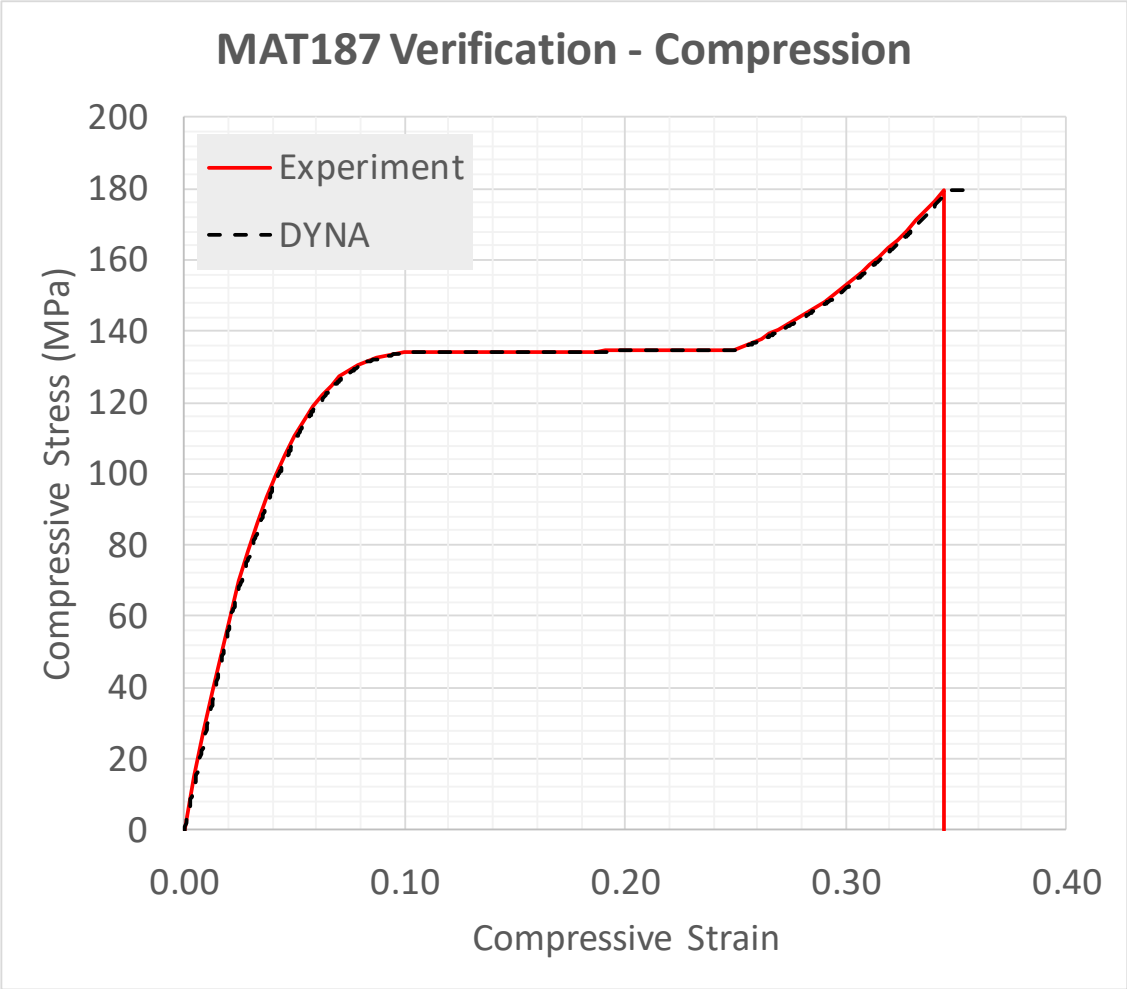

6.11 Compression Single-Element Stress vs. Strain Plot for Deformation Only

Figure 6.12 shows the longitudinal stress vs. strain curve for the compression single element with deformation and failure.

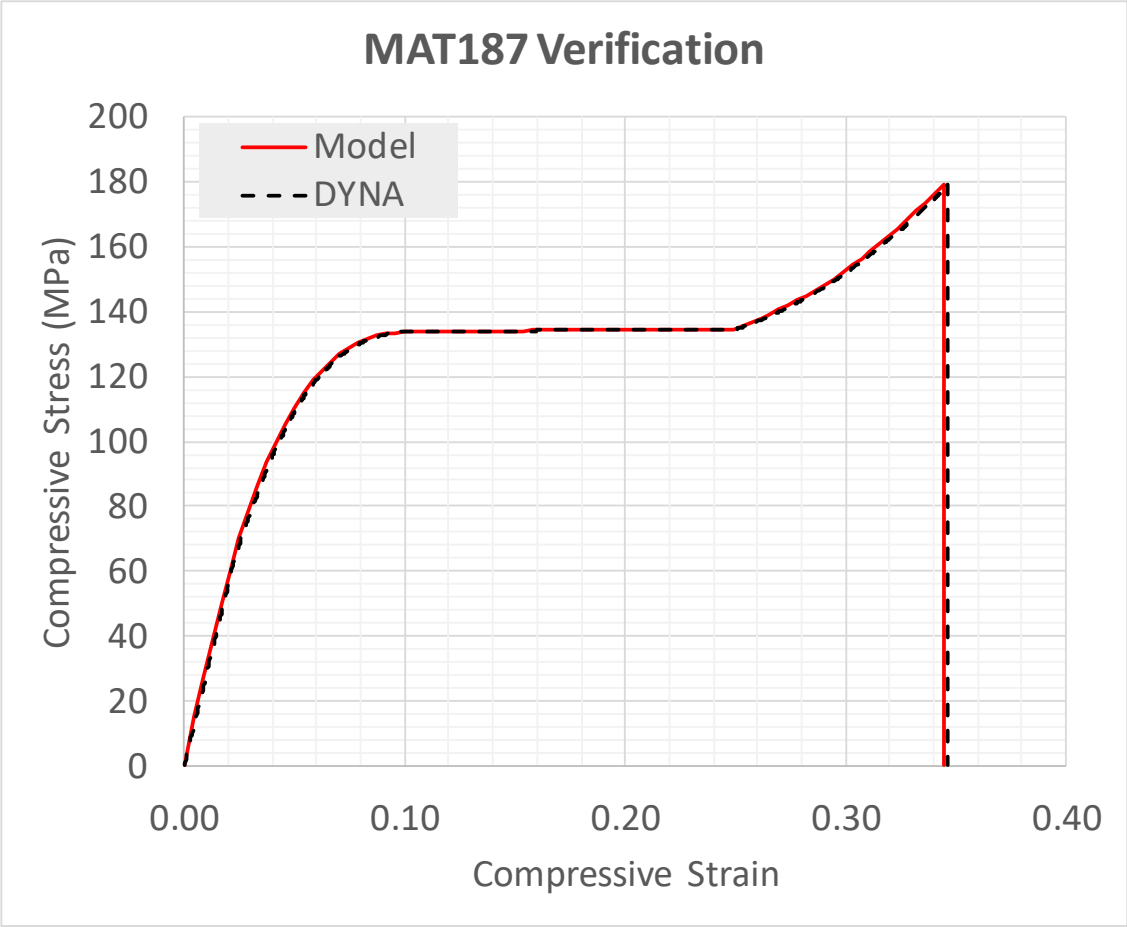

6.12 Compression Single-Element Stress vs. Strain Plot for Deformation and Failure

Figure 6.13 shows the shear stress vs. strain curve for the shear single element with deformation only.

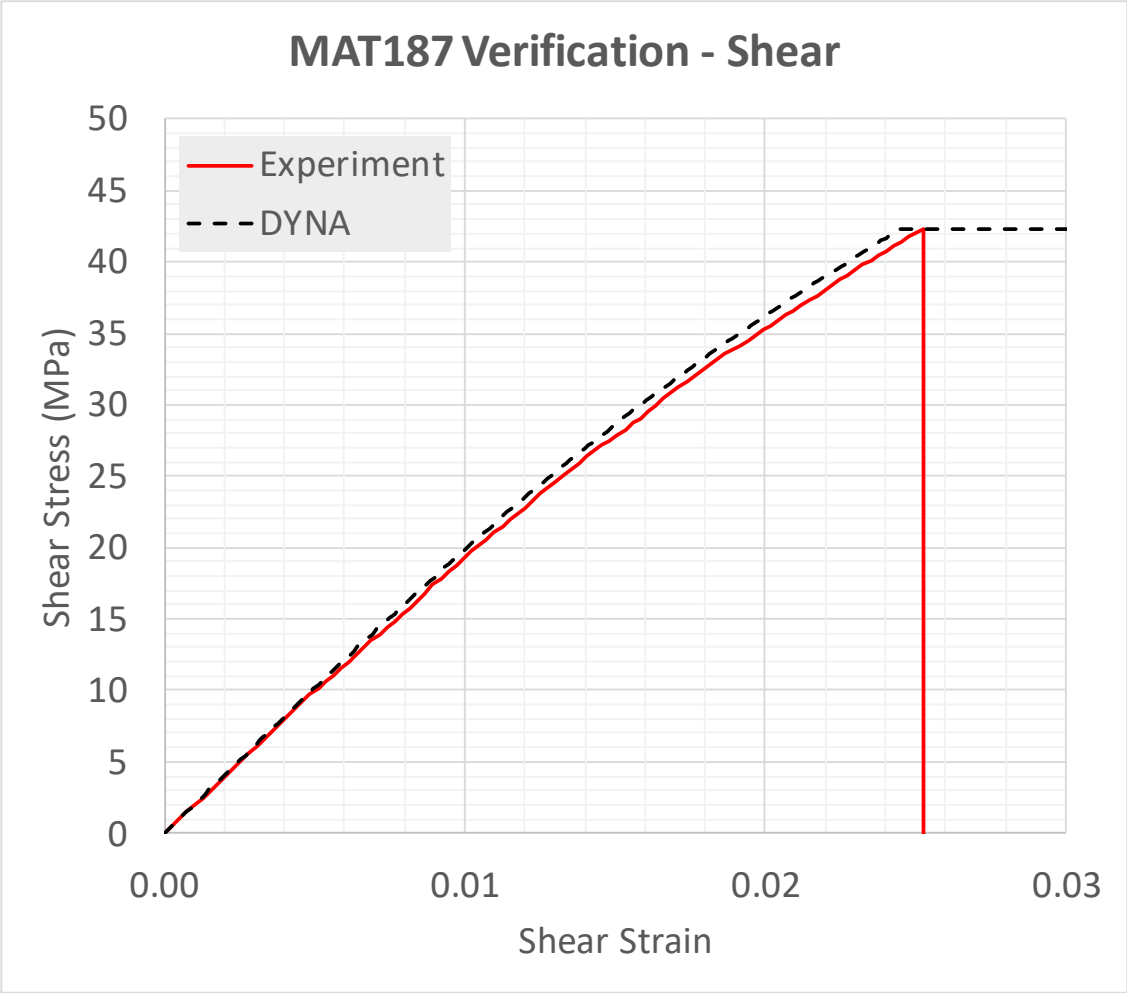

6.13 Shear Single-Element Stress vs. Strain Plot for Deformation Only

Figure 6.14 shows the shear stress vs. strain curve for the shear single element with deformation and failure.

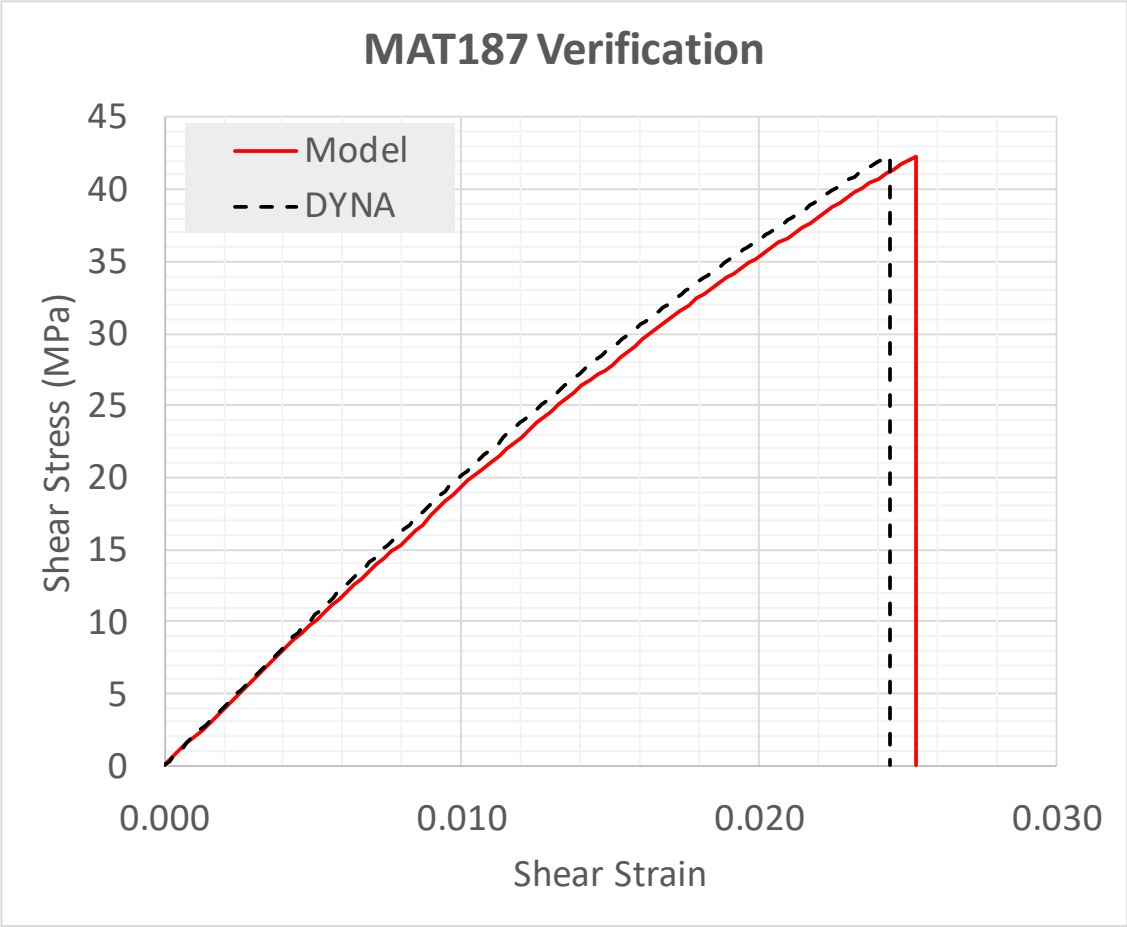

6.14 Shear Single-Element Stress vs. Strain Plot for Deformation and Failure

6.4.3 Discussion

The deformation simulations correlated well between the experiment and simulations. In both the tension and compression simulations, the stress vs. strain curves lie almost on top of one another with a root mean square error (RMSE) of 0.09 MPa and 1.14 MPa respectively which corresponds to less than a percent difference from the average stress value. The shear simulation shows a difference in the deformation where the simulation does not yield as early as the experiment and results in a stiffer response. With a RMSE of 0.65 between the curves which is greater than a percent difference but still within a reasonable margin of error.

When failure was turned on using the values discussed above, the results are almost identical. The tension and compression deformation curves are almost identical to the experimental curves with the shear curve having a slight stiffness increase compared to the experiment. The failure point for the tension is 0.1% lower than the experiment in terms of strain and 0.1% lower in terms of stress. The failure point of the compression test is 0.1% higher in terms of strain compared to the experiment and 0.1% lower in terms of stress. The shear test was 2.3% lower in terms of strain when compared to the experiment and 0.1% higher in terms of stress. These differences are numerically insignificant and indicates that the failure predicted by the material model is accurate.

6.5 LS-DYNA Simulation of F3900 Matrix Tension

6.5.1 Simulation Modeling

The tension multi-element simulation was modeled using the entire specimen and utilizing the geometry prescribed in ASTM D638-14 (2014) and using the same dimensions used for the experiment. No planes of symmetry were utilized in this simulation. The boundary conditions prescribed were one end of the specimen entirely fixed in all three global axes with the other end fixed in the Y and Z directions with the nodes moving in the X direction. The nodes that were fixed were chosen to emulate the boundary conditions of the experiment where all nodes in the “tab” region were fixed at either end. The model was meshed in such a way to preserve the overall shape of the specimen while also reducing the number of distorted elements and keeping the element aspect ratios close to or equal to 1.0. The details of the model can be found in table 6.2. Three elements were used through the thickness of the model.

6.2. Tension Multi-Element Model Details

Number of Elements	Number of Nodes	Max Aspect Ratio	Min Aspect Ratio
5976	8684	1.60	1.23

6.5.2 Results

Figure 6.15 shows the region analyzed for all post processing of the multi-element tensile tests.

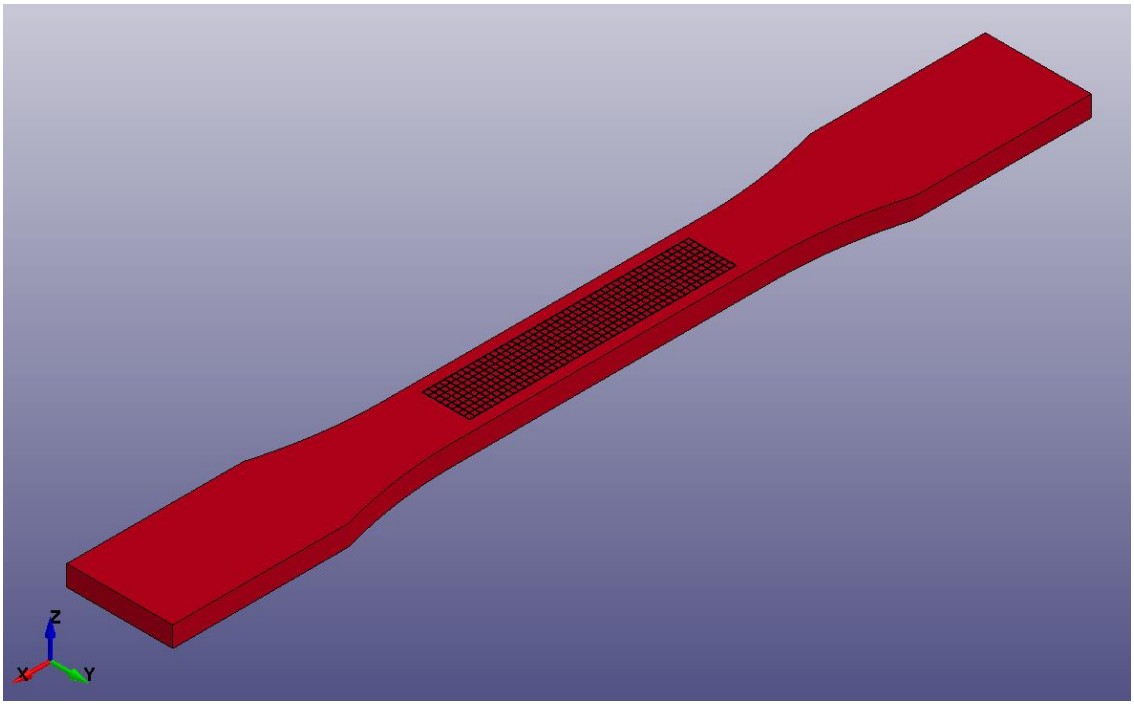

6.15 Tension Multi-Element Analysis Region

Figure 6.16 shows the longitudinal stress vs. strain plot for the tension multi-element test with deformation only.

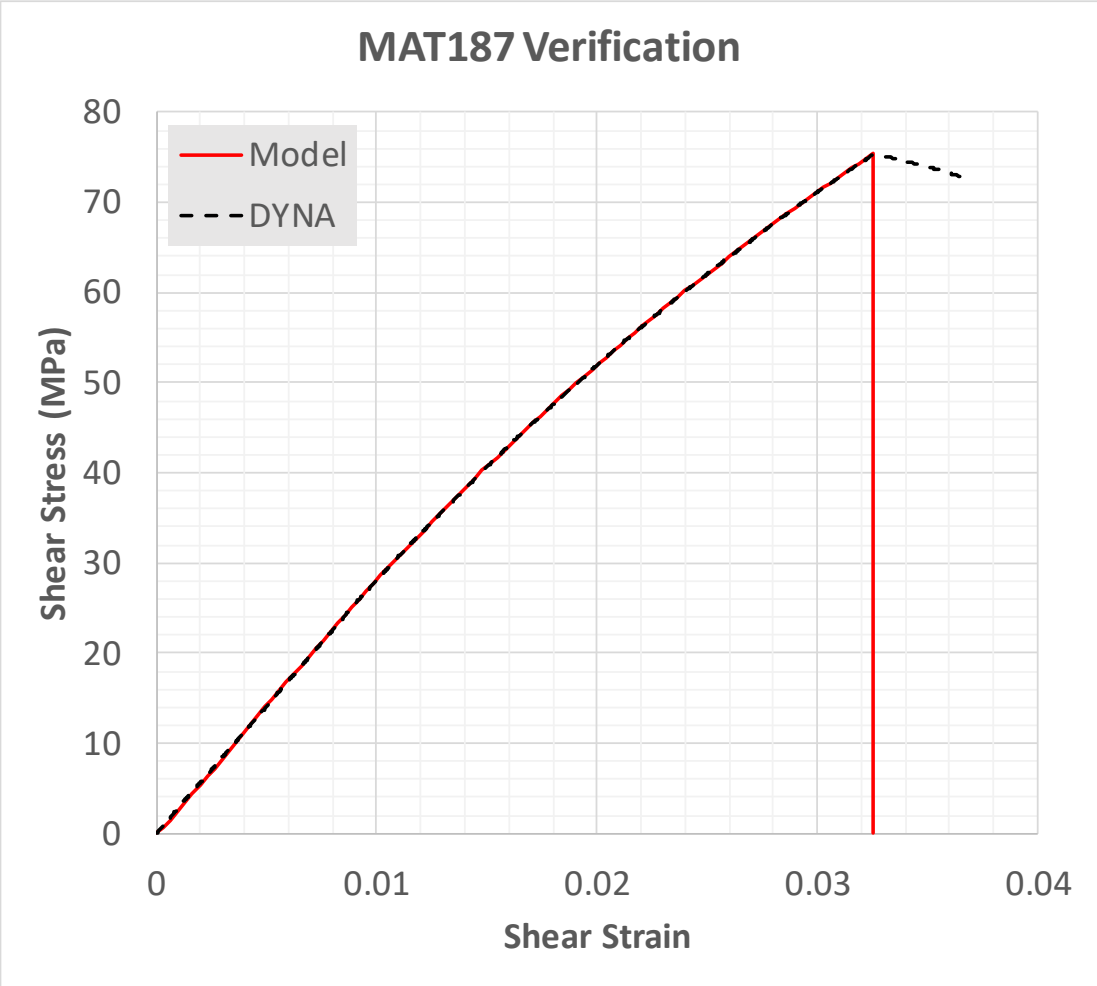

6.16 Tension Multi-Element Stress vs. Strain Plot for Deformation Only

Figure 6.17 shows the longitudinal stress vs. strain plot for the tension multi-element test with deformation and failure.

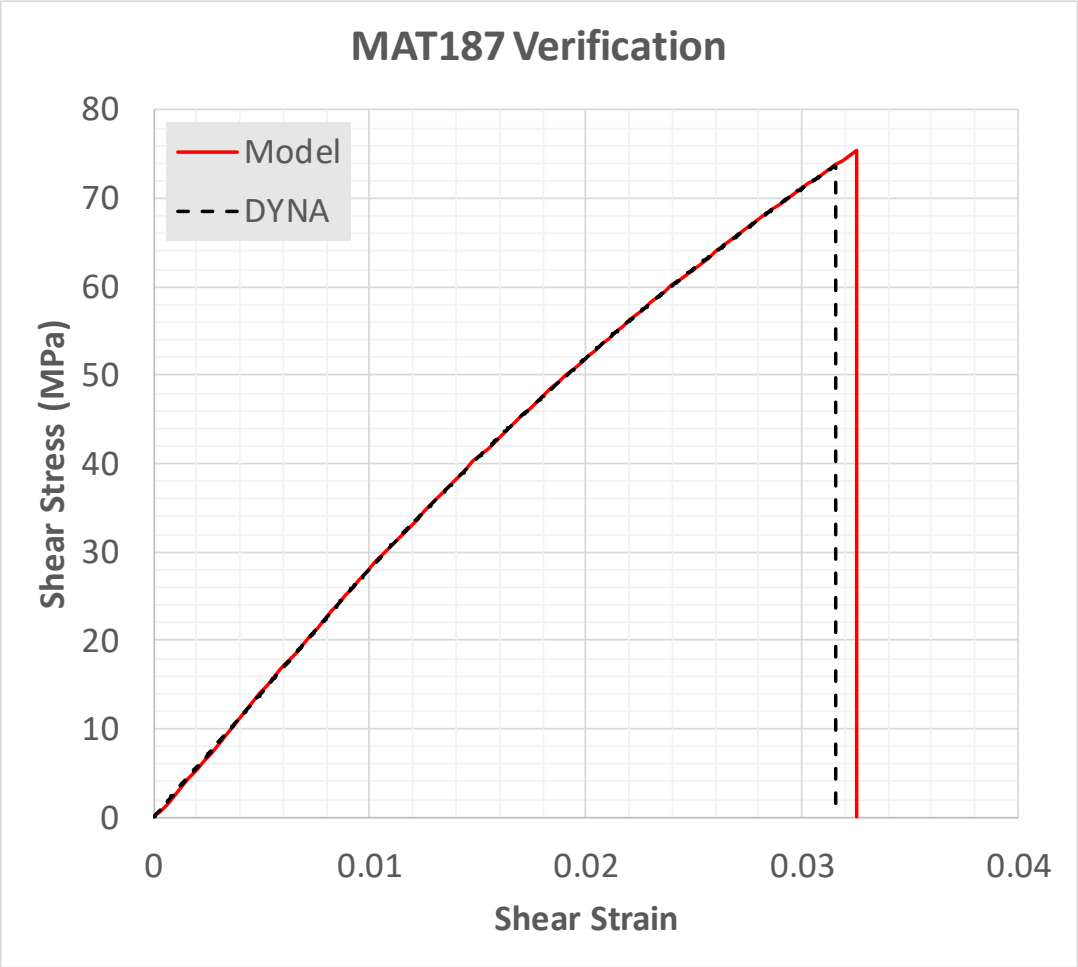

6.17 Tension Multi-Element Stress vs. Strain Plot for Deformation and Failure

Figure 6.18 shows the energy check plot the tension multi-element test with deformation only.

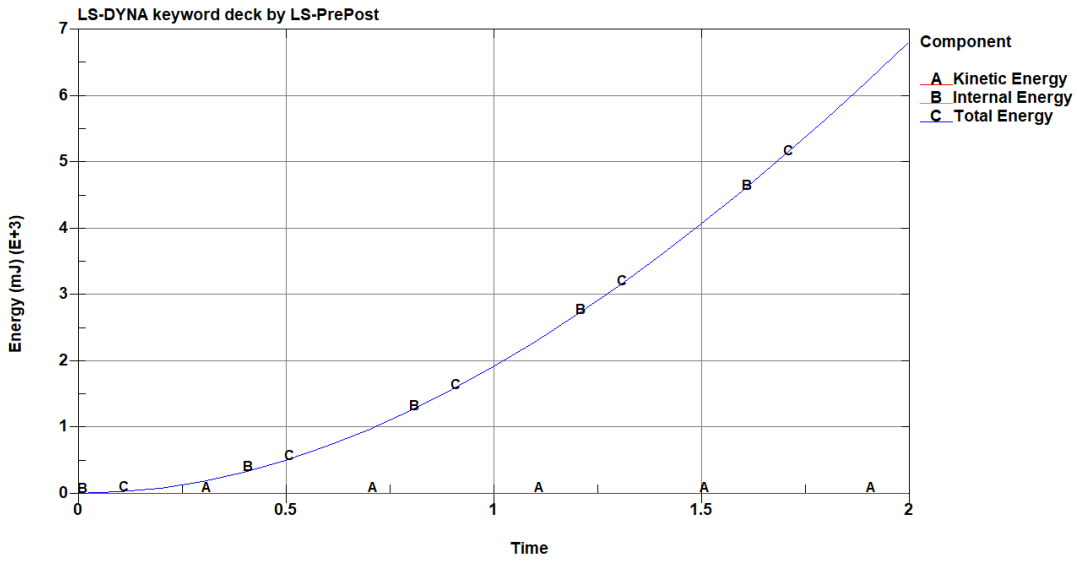

6.18 Tension Multi-Element Energy Check Plot

6.5.3 Discussion

Similarly, to the single element test, the tensile multi-element test behaves almost exactly as the experiment when comparing the longitudinal stress and strain. The RMSE between the curves is only 0.10 MPa. This provides confidence in the material model as well as the boundary conditions and model geometry. Figure 6.19 shows the fringe plot for the X-strain (longitudinal) alongside the X-strain from the DIC plot for a representative replicate. From the comparison one can see that the two share a similar strain field with similar strain distributions at the change in geometry of the specimen. This provides confidence in the assumptions that both the specimen was under pure tension as well as the fact that the model replicates the conditions of the test accurately. The energy for the simulation also shows almost no kinetic energy in the simulation with the total and internal energy curves being on top of one another. This provides confidence that the rate of loading for the test does induce any dynamic effects.

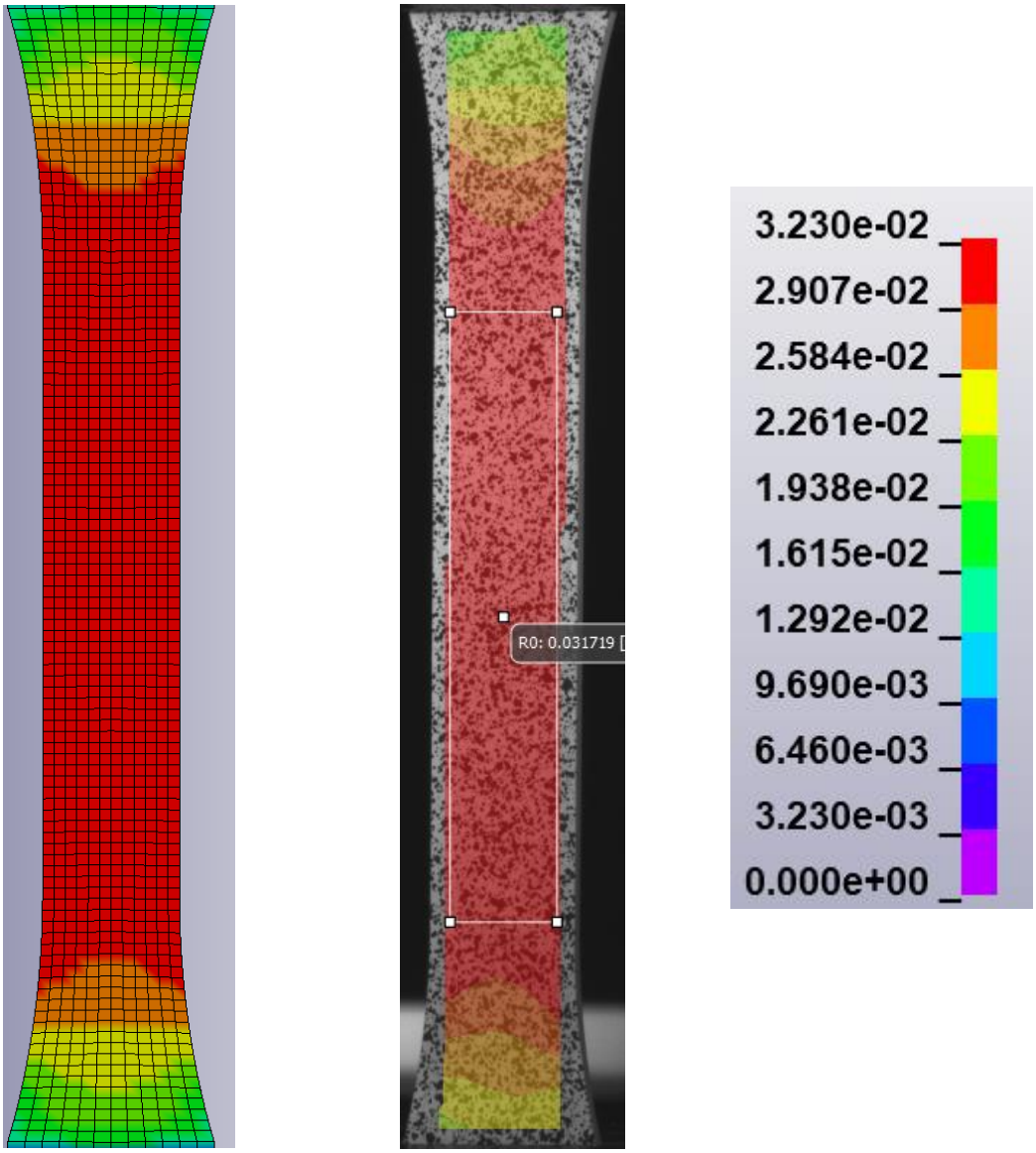

(a) (b)

6.19 Longitudinal Strain Plot for (a) LS-DYNA Simulation and (b) Experimental Results

When failure was included, the results are consistent with previous simulations. The failure point when using the previous outlined variables was observed to be 3.8% lower in terms of strain and 2.7% lower in terms of stress. This provides confidence in the material model as well as the parameters calibrated in the single element verification tests with regards to failure.

6.6 LS-DYNA Simulation of F3900 Matrix Compression

6.6.1 Simulation Modeling

For this simulation the gage section was modelled and a quarter symmetry was utilized about the global XZ and XY planes. The specimen dimensions were taken to be the same as the experiment with a gage section of 12.7 mm, specimen width of 12.7 mm, and an overall thickness of 4.00 mm. These dimensions were reduced to a specimen width of 6.35 mm and an overall thickness of 2.00 mm when using the quarter model. The boundary conditions used were: the nodes on the planes of symmetry were fixed in the direction perpendicular to that plane (XZ was fixed in the Y and XY was fixed in the Z), the nodes on one end were fixed in all three global directions, and the nodes on the other end were fixed in just the YZ directions and were loaded in the X direction. The specimen was meshed in such a way that elements were not distorted and the aspect ratio was kept as close to 1.0 as possible. The details of the model are shown in table 6.3.

6.3 Compression Multi-Element Model Details

Number of Elements	**Number of Nodes**	**Max Aspect Ratio**
1352	1890	1.05

6.6.2 Results

Figure 6.20 shows the region analyzed for all post processing of the multi-element compression tests.

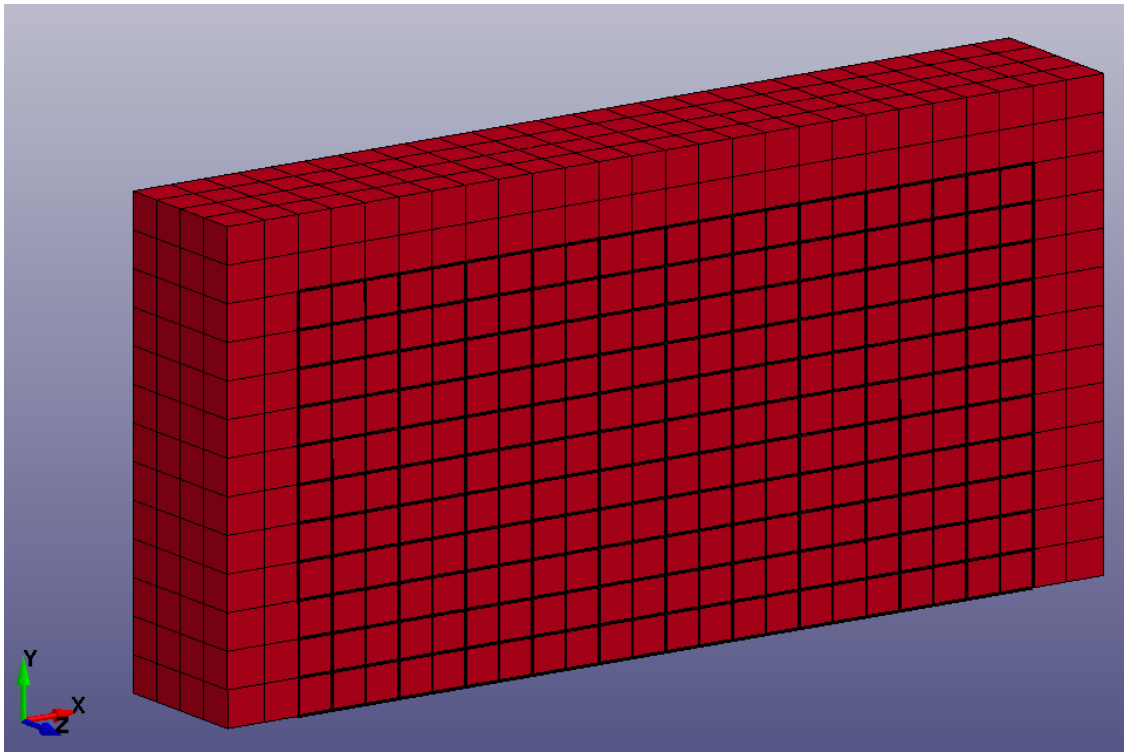

6.20 Compression Multi-Element Analysis Region

Figure 6.21 shows the longitudinal stress vs. strain plot for the compression multi-element test with deformation only.

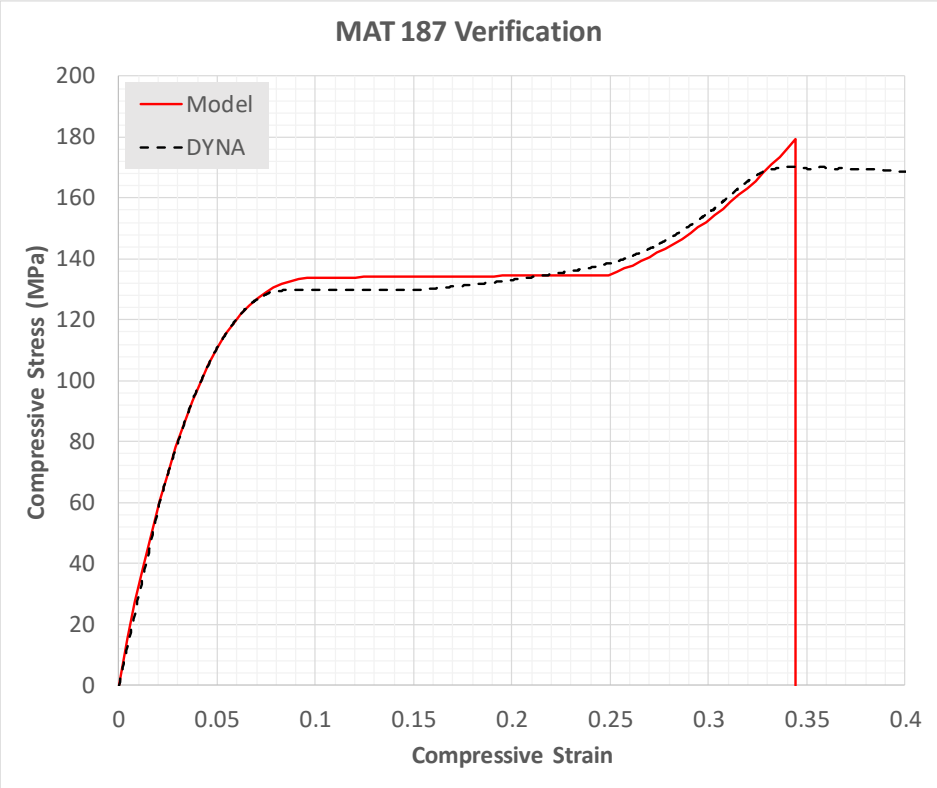

6.21 Compression Multi-Element Stress vs. Strain Plot for Deformation Only

Figure 6.22 shows the longitudinal stress vs. strain plot for the compression multi-element test with deformation and failure.

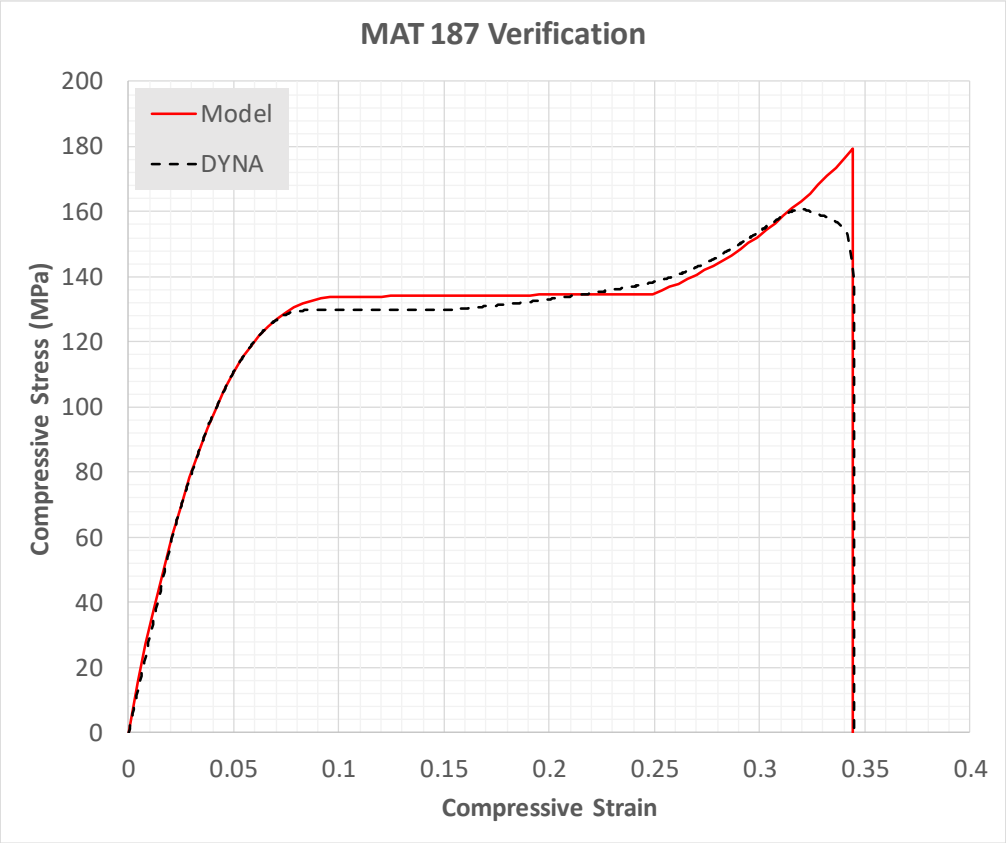

6.22 Compression Multi-Element Stress vs. Strain Plot for Deformation and Failure

Figure 6.23 shows the energy check plot the compression multi-element test with deformation only.

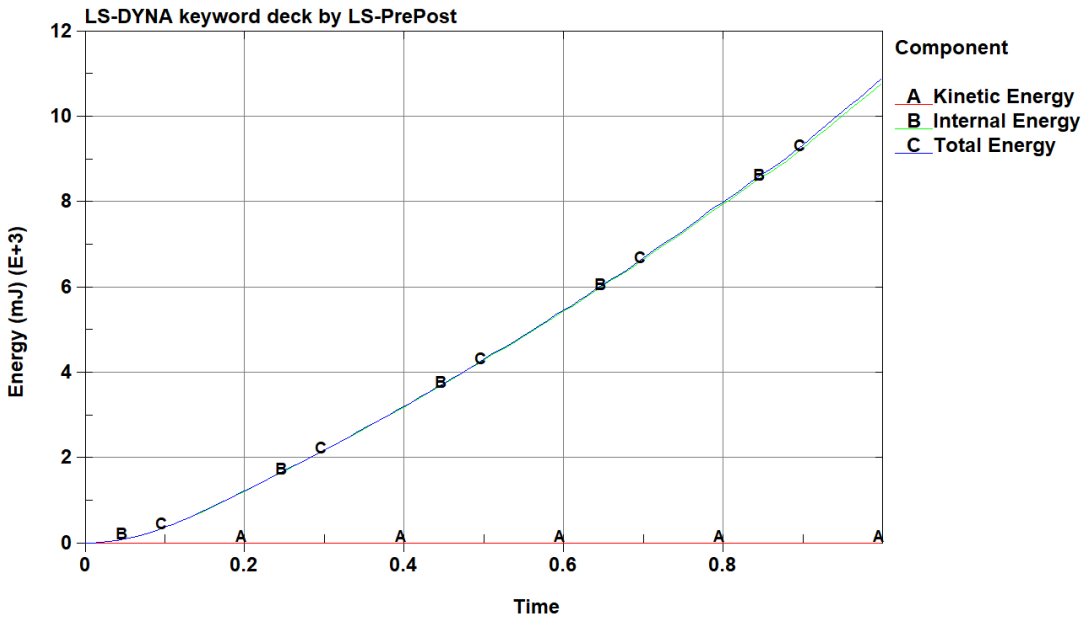

6.23 Compression Multi-Element Energy Check Plot

6.6.3 Discussion

The compression multi-element test follows the experimental model curve similarly to the single element test until a strain value of approximately 0.05. At this point the average response plateaus at a stress value of approximately 129 MPa which is 3% lower than the prescribed input of 133 MPa. From there the response follows the experimental curve and reaches a peak stress value of 170 MPa before levelling of and reaching apparently reaching the end of the input curve. When failure is enabled the elements toward the middle of the model fail first which causes the initial decrease in strength and then elements through the center of the model fail and cause the specimen to no longer be able to carry load. The difference in strain is approximately 0.1% whereas the stress is approximately 10% with an RMSE value of 2.9 MPa for the deformation only simulation and a value of 6.1 MPa when failure is enabled. This increase is caused by the region between 0.3 and 0.35 strain where the elements begin to fail. However the

simulation does provide confidence that the calibrations to RBCFAC and DEPRPT are sufficient for modeling the deformation and failure of the multi-element compression specimen.

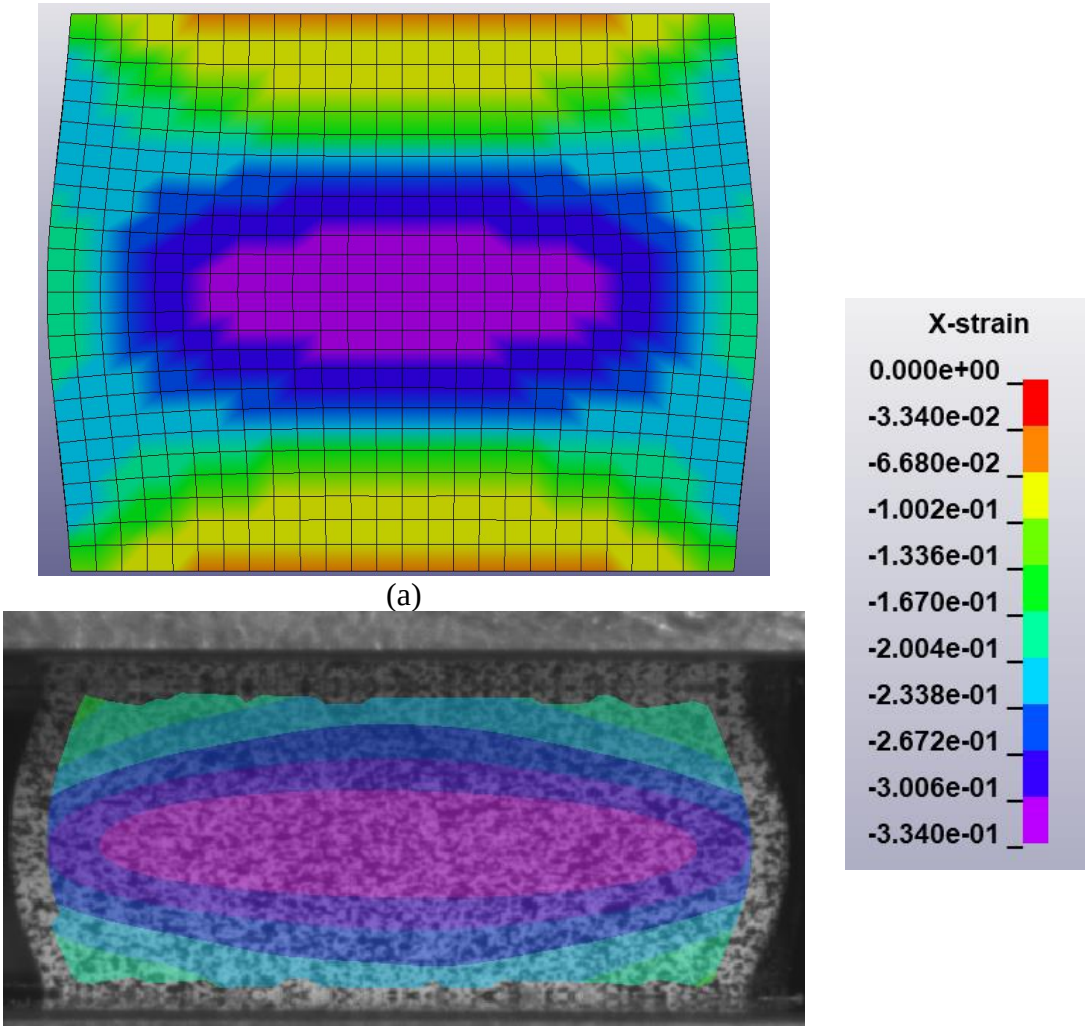

6.24 Longitudinal Strain Plot for Compression (a) LS-DYNA Simulation and (b) Experimental DIC Plot

6.7 LS-DYNA Simulation of F3900 Matrix V-Notch Shear

6.7.1 Simulation Modeling

The simulation for the multi-element shear test was done in such a way that it mimicked the experiment as closely as possible. In order to do this the fiberglass tabs

needed to be modeled as well. This was done using a purely elastic material model (MAT001) and using publicly available material properties for the G10 fiberglass. These are shown in Table 6.4

6.4 G10 Fiberglass Material Properties

Modulus of Elasticity	**Poisson's Ratio**	**Density**
2700 ksi	0.12	2.02e-3 slug/in^3

The two materials were also assumed to be rigidly affixed to one another and shared the same nodes. This is because no influence on the strength of the bond was observed except that it was greater than the strength of the F3900 matrix itself and thus did not need to be modeled since the material would fail before the bond between the matrix and the fiberglass tab. The boundary conditions were formulated in such a way that the actual boundary conditions were observed. Based on figure 4.3.2 one can see that the specimen is not completely fixed on both top and bottom faces, that the top left and bottom right faces have a reduced point of contact keeping them fixed. This would cause the difference in strain fields observed as well as the failure originating from the two more rigidly affixed corners. The nodes that were fixed were done to best approximate this condition and both ends of the specimen were fixed in the X direction and loaded in the Y direction. The mesh was created in such a way that the mesh was uniform and elements were not distorted and maintained an aspect ratio as close to 1.0 as possible. The details of the mesh for the matrix only can be found in table 6.5. Two elements were used through the thickness for the matrix and only one for each of the four fiberglass tabs.

6.5 Shear Multi-Element Model Details

Number of Elements Matrix	Number of Elements Tabs	Number of Nodes	Max Aspect Ratio	Min Aspect Ratio
2184	1848	5594	2.55	1.92

6.7.2 Results

Figure 6.25 shows the region analyzed for all post processing of the multi-element shear test.

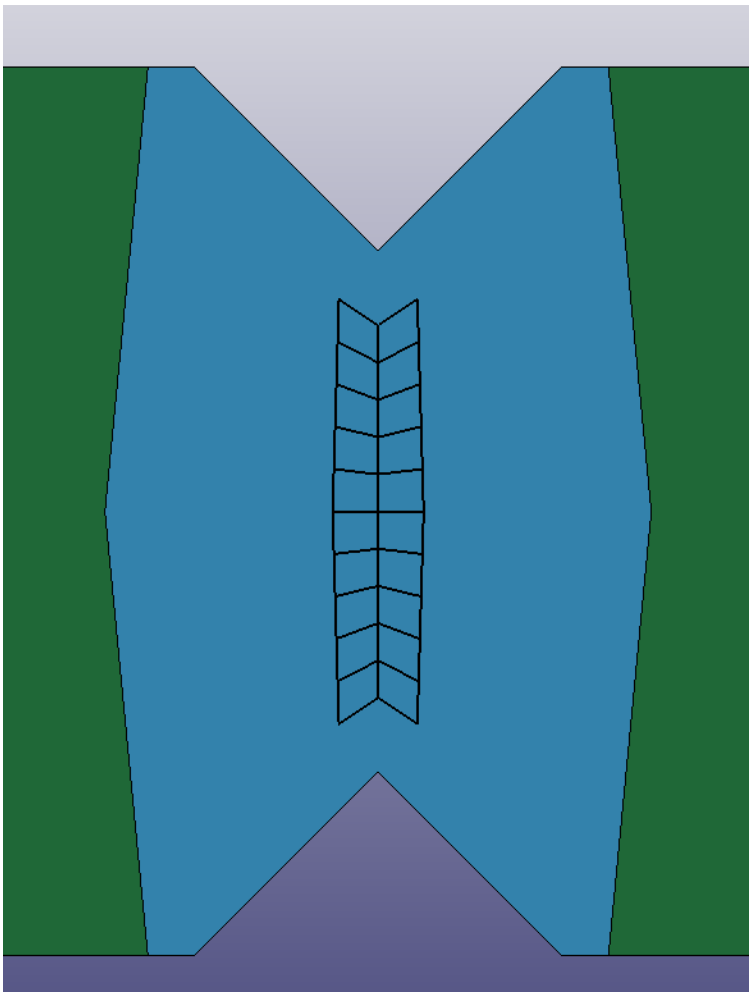

6.25 Shear Multi-Element Analysis Region

Figure 6.26 shows the longitudinal stress vs. strain plot for the shear multi-element test with deformation only.

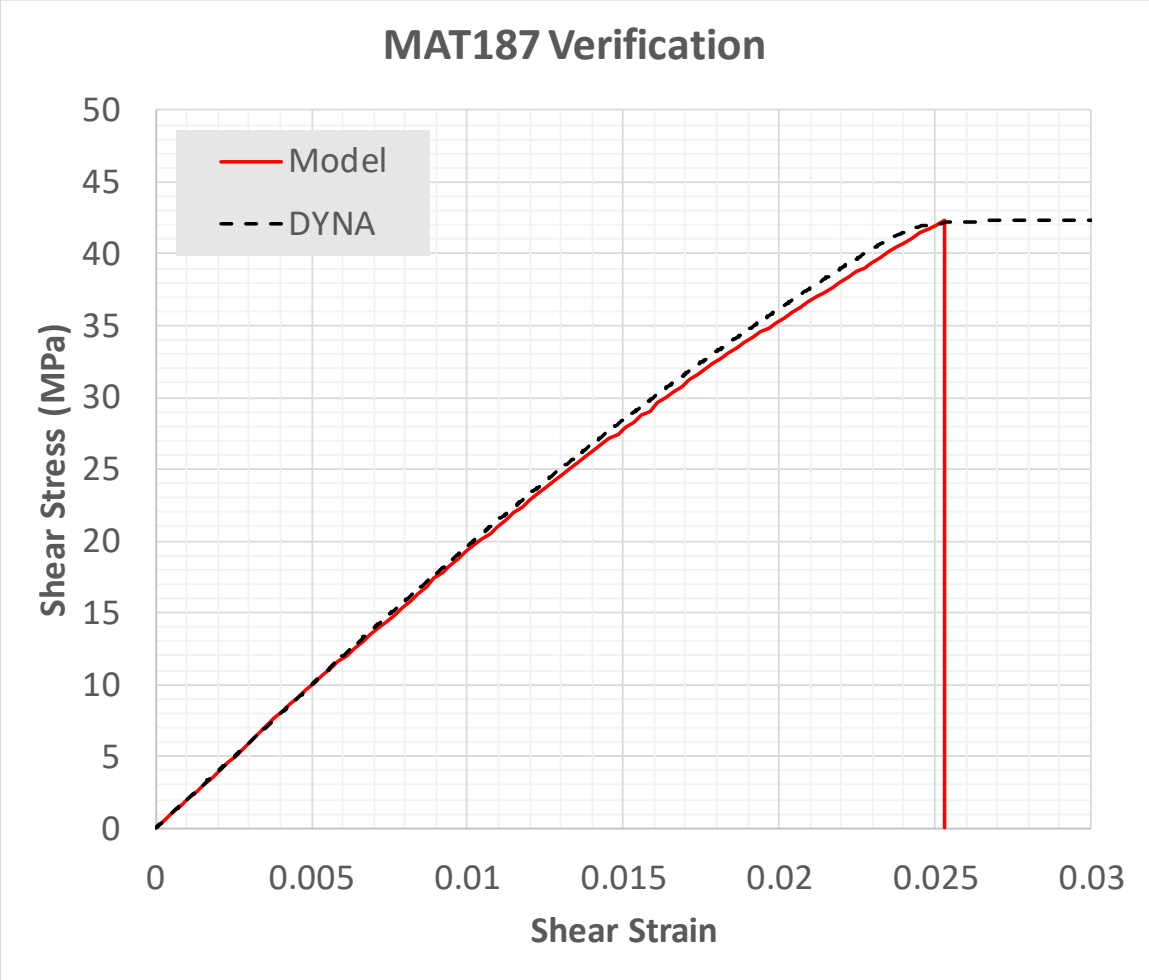

6.26 Shear Multi-Element Stress vs. Strain Plot for Deformation Only

Figure 6.27 shows the longitudinal stress vs. strain plot for the shear multi-element test with deformation and failure.

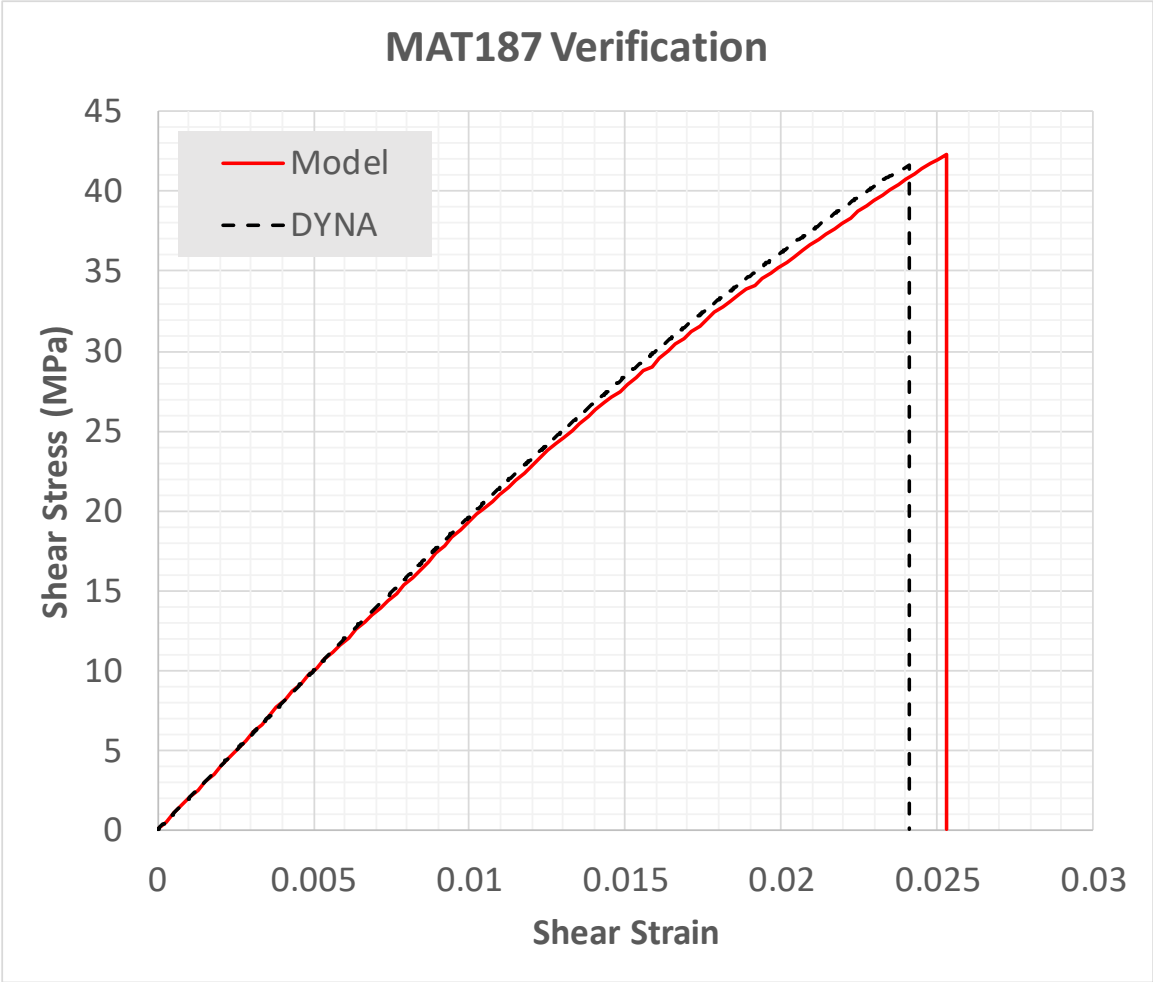

6.27 Shear Multi-Element Stress vs. Strain Plot for Deformation and Failure

Figure 6.28 shows the energy check plot the shear multi-element test with deformation only.

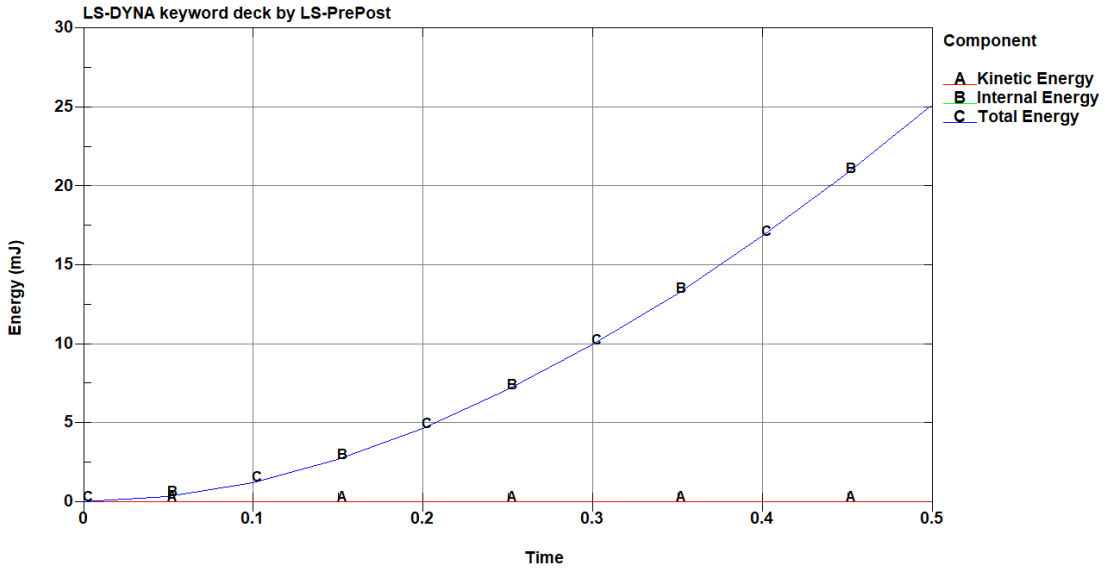

6.28 Shear Multi-Element Energy Check Plot

6.7.3 Discussion

Similar to the single element verification test the shear deformation shows a slightly stiffer response in the plastic region with a RMSE between the curves of 1.06 MPa. When failure is enabled the difference in the strain and stress is similar to the single element as well with the stress being approximately 1.7% lower than the experiment and the strain being 4.6% lower than the experiment. However the elements that are failing are the elements along the centerline of the specimen, in the analysis region. During the experiment, when the specimen failed, it was in two diagonal lines connecting the more restrictive corners of the gage section. This suggests that current failure parameters are accurate in predicting the overall failure values of the specimen but more calibration would need to be made to the failure parameters in order to promote a failure pattern similar to the experiment.

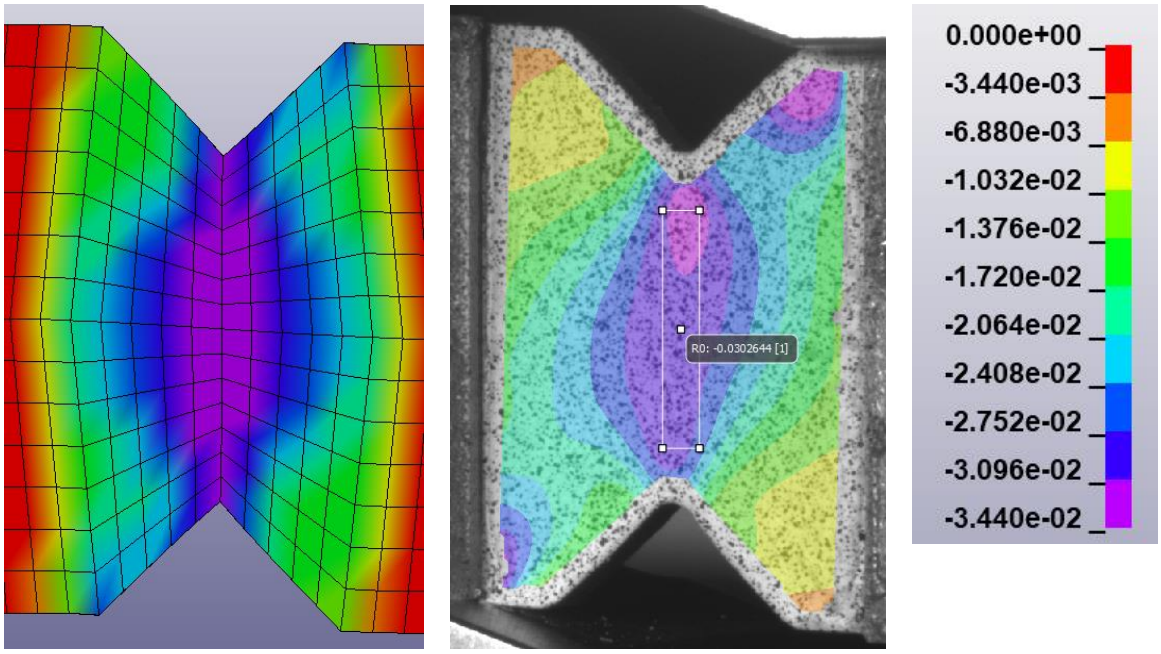

(a) (b)

6.29 Shear Strain Field for (a) LS-DYNA Simulation and (b) Experimental DIC Plot

When failure is enabled, the specimen fails earlier than the experiment at a strain 33% lower than the experiment and at a stress value 26% lower. This reduction in stress and strain is similar to the compression multi-element test which suggest that the elements are not in a state of pure compression or shear stress. For the shear test, figure 6.30 shows the pressure vs. von mises plot along with the differentiated plot generated by LS-Dyna showing the average triaxiality of the elements. This shows a non-zero value which means the elements are not in a state of pure shear which would cause the incorrect failure strain. This would also mean that other plastic strains are developing which would increase the effective plastic strain of the elements and would cause the failure point to occur earlier than was observed in the experiment.

7. Concluding Remarks

This report summarized the experimental characterization of the F3900 Epoxy Matrix as well as the tensile characterization of the T800s Carbon Fiber. The material model MAT187 was then calibrated using the experimental results to emulate the F3900 matrix in a finite element analysis including both deformation and failure. The ultimate strength in tension, compression, and shear was determined to be 10 580 psi, 25 900 psi, and 5 940 psi respectively. The carbon fiber was found to have a peak stress value of 309 000 psi.

The tensile test and the v-notch shear test of the epoxy matrix showed slight plasticity before ultimately failing in a brittle fashion with a sudden complete loss of load carrying capacity. The compression test of the epoxy however exhibited a significant plasticity with some stress cracking before the test was terminated due to complete loss in strain data.

The major stresses and strains were accurately captured and calibrated for as well as the overall strain field when compared to the experimental results. The failure was also accurately replicated with there being about a0 3% maximum difference in the peak strain and stress between the simulation and the experiment. The RMSE of these simulations was also between 0.1% and 5% of the average stress value of the experiment.

REFERENCES

Adams, Donald, W., Jeffry. (1997). The Wyoming Combined Loading Compression (CLC) Test MEthod. *Joudnal of Composites Technology & Research*, *19*(3), 123–133.

C28 Committee. (n.d.). *Test Method for Tensile Strength and Youngs Modulus of Fibers*. https://doi.org/10.1520/C1557-14

Correlated Solutions Inc. (2016). Retrieved July 10, 2019, from http://correlateedsolutions.com/vic-3d/

D20 Committee. (n.d.-a). *Test Method for Compressive Properties of Rigid Plastics*. https://doi.org/10.1520/D0695-15

D20 Committee. (n.d.-b). *Test Method for Shear Strength of Plastics by Punch Tool*. https://doi.org/10.1520/D0732-17

D20 Committee. (n.d.-c). *Test Method for Tensile Properties of Plastics*. https://doi.org/10.1520/D0638-14

D30 Commitee. (1975). *D3379-75 Standard Test Method for Tensile Strength and Young's Modulus for High Modulus Single Filament Materials*. https://doi.org/10.1520/D3379-35R89E01

D30 Committee. (n.d.). *Test Method for Shear Properties of Composite Materials by the V-Notched Beam Method*. https://doi.org/10.1520/D5379_D5379M-12

Goyal, S., Karthik, V., Kasiviswanathan, K. V., Valsan, M., Rao, K. B. S., & Raj, B. (2010). Finite element analysis of shear punch testing and experimental validation. *Materials & Design (1980-2015)*, *31*(5), 2546–2552. https://doi.org/10.1016/j.matdes.2009.11.031

Kim, J., McDonough, W. G., Blair, W., & Holmes, G. A. (2008). The Modified-single fiber test: A methodology for monitoring ballistic performance. *Journal of Applied Polymer Science*, *108*(2), 876–886. https://doi.org/10.1002/app.27684

Kolling, S., Haufe, A., Feucht, M., & Dubois, P. (2005). *SAMP-1: A Semi-Analytical Model for the Simulation of Polymers.*

Langston, T. A., & Granata, R. D. (2014). Influence of nitric acid treatment time on the mechanical and surface properties of high-strength carbon fibers. *Journal of*

Composite Materials, *48*(3), 259–276. https://doi.org/10.1177/0021998312470471

Littell, J. (2008). *The Experimental and Analytical Characterization of the Macromechanical Response for Triaxial Braided Composite Materials* (University of Akron). Retrieved from http://rave.ohiolink.edu/etdc/view?acc_num=akron1224164770

Liu, K., & Piggott, M. R. (1995). Shear strength of polymers and fibre composites: 1. thermoplastic and thermoset polymers. *Composites*, *26*(12), 829–840. https://doi.org/10.1016/0010-4361(95)90876-2

Prepared by LS-DYNA Aeorspace Working Group. (2018, November 5). *MAT_224 Dynamic Punch Test Aluminium 2024*.